Journal of Medicinal Chemistry

Article

Large-Scale Validation of a Quantum Mechanics Based Scoring Function: Predicting the Binding Affinity and the Binding Mode of a Diverse Set of Protein–Ligand Complexes

Kaushik Raha, and Kenneth M. Merz

J. Med. Chem., **2005**, 48 (14), 4558-4575• DOI: 10.1021/jm048973n • Publication Date (Web): 21 June 2005

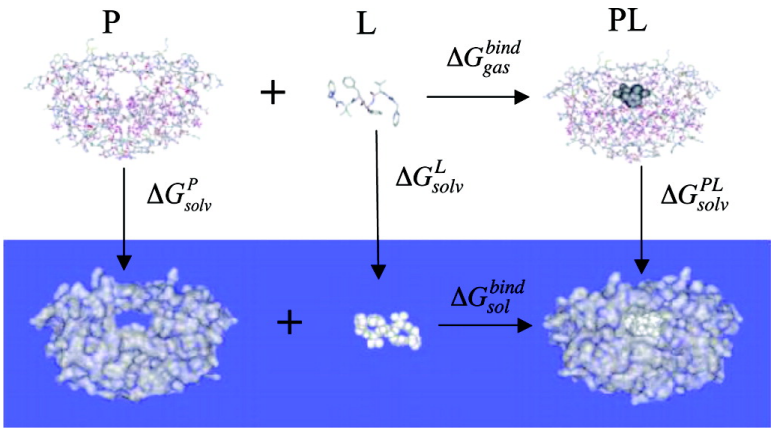

More About This Article

Additional resources and features associated with this article are available within the HTML version:

- Supporting Information
- Links to the 12 articles that cite this article, as of the time of this article download
- Access to high resolution figures
- Links to articles and content related to this article
- Copyright permission to reproduce figures and/or text from this article

View the Full Text HTML

Journal of Medicinal Chemistry is published by the American Chemical Society. 1155 Sixteenth Street N.W., Washington, DC 20036

Large-Scale Validation of a Quantum Mechanics Based Scoring Function: Predicting the Binding Affinity and the Binding Mode of a Diverse Set of Protein−Ligand Complexes

Kaushik Raha[†] and Kenneth M. Merz, Jr.*

Department of Chemistry, 104 Chemistry Building, The Pennsylvania State University, University Park, Pennsylvania 16802

Received December 20, 2004

Computational methods to calculate binding affinity in protein−ligand interaction are of immense interest because of obvious practical applications in structure-based drug design. Scoring functions attempt to calculate the variation in binding affinity of ligands−inhibitors bound to protein targets at various levels of theory. In this study we use semiempirical quantum mechanics to design a scoring function that can calculate the electrostatic interactions and solvation free energy expected during complexation. This physically based approach has the ability to capture binding affinity trends in a diverse range of protein−ligand complexes. We also show the predictive power of this scoring function within protein targets and its ability to score ligand poses docked to a protein target. We also demonstrate the ability of this scoring function to discriminate between native and decoy poses and highlight the crucial role played by electrostatic interactions in molecular recognition. Finally we compare the performance of our scoring function with other available scoring functions in the literature.

Introduction

The chemistry and physics associated with protein−ligand interaction has been an area of active research with widespread implications for structure-based design of small-molecule inhibitors. There is relentless pressure on the pharmaceutical industry to reduce costs because of the extreme difficulty in bringing a compound to the market as a drug.[1] In silico virtual screening has been a very attractive and cost-effective alternative to experimental screening because of its ability to screen a large number and broad range of compounds.[2,3] In this process a database of compounds are docked to a receptor binding site and then a docked "pose" is scored on the basis of a potential function that describes the relationship between the structure of the complex and the free energy of binding. This has been a very popular procedure to identify possible lead compounds. In some cases docking algorithms have been reasonably successful in predicting binding modes; however, scoring the poses to predict the binding affinity has proved to be more challenging.[4−6] The potential functions used in docking and scoring are referred to as "scoring functions". Present day scoring schemes are too simplistic and sacrifice quality for speed, or they are too detailed and time-consuming for practical applications.[7,8] Moreover, the time-consuming methods that use molecular simulation,[9] by their very nature, have made large-scale validation a challenge. Thus, despite all the recent developments in this area, a physically satisfying model that is robust enough to satisfactorily evaluate the binding of ligands to proteins accurately in a reasonable amount of time has proven to be elusive. In general, the scoring functions that have been used can be divided into three categories: physical−chemical, empirical, and knowledge based potentials. Recently we have reviewed binding free energy calculation protocols and different scoring functions in greater detail.[10]

Quantum mechanics (QM), though not new to the field of molecular interaction, has till now been used only to study smaller chemical and biochemical systems because of the exorbitant computational costs associated with this approach. In recent work from our group we have reported the development of a linear scaling methodology that uses the divide and conquer (D&C) approach for solving large molecular systems with QM.[11−13] This method has been implemented in our computer program DivCon[14] and uses the semiempirical Hamiltonians (AM1,[15] PM3,[16] MNDO/d,[17,18] or PM3-PDDG[19]) to solve the Schrödinger equation for large biomolecular systems. The use of QM also allows us to move away from force field based methods especially for evaluating electrostatic interactions. Monopole−monopole interactions calculated using force field based methods represent a significant approximation to electrostatic interaction and are generally designed to treat QM effects in an average manner. QM effects, like polarization and charge transfer, are either embedded into the monopolar approximation or added via extra parametrized terms.

Energy decomposition studies that we have carried out using semiempirical linear scaling calculations have shown that solvent induces a significant polarization on the protein electron density that can enhance or reduce the interaction between a ligand and protein-based receptor.[20] Perez and Ortiz have used linear discriminant analysis and concluded that a sophisticated treatment of desolvation and hydrogen bond interactions is important in scoring functions.[21] Charge transfer effects are especially pronounced in metalloenzyme−ligand

* To whom correspondence should be addressed. 1 Phone: 814-865-3623. Fax: 814-865-3292. E-mail: merz@psu.edu.

[†] Integrative Biosciences Graduate Program, The Huck Institute of Life Sciences, The Pennsylvania State University, University Park, PA 16802.

10.1021/jm048973n CCC: $30.25
Published on Web 06/21/2005

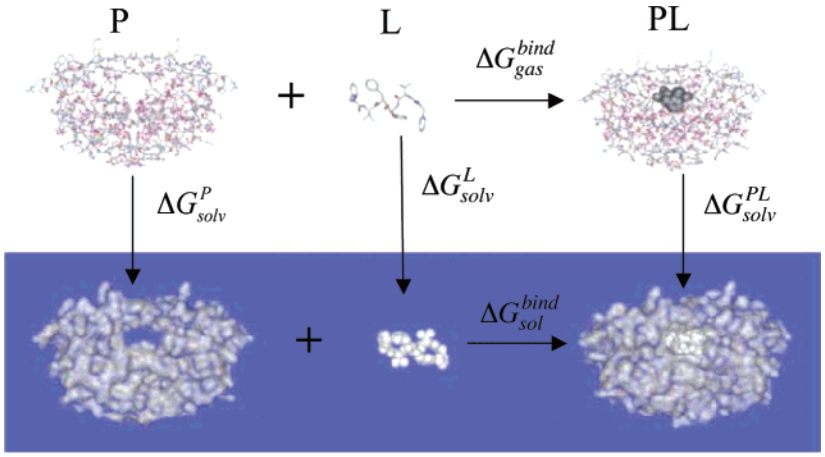

Figure 1. Thermodynamic cycle used to calculate the free energy of binding in solution between the protein and ligand during complexation. ΔG^{P}_{solv} is the solvation free energy of protein, ΔG^{L}_{solv} is the solvation free energy of the ligand, and ΔG^{PL}_{solv} is the solvation free energy of the protein−ligand complex. ΔG^{bind}_{gas} is the free energy of binding in the gas phase, and ΔG^{bind}_{sol} is the free energy of binding in solution.

complexes. We have shown such effects to be significant in previous studies.[22] Hence, predicting binding affinities using classical force field based methods faces many hurdles.

Recently, we introduced a QM-based scoring function to predict the free energy of binding in protein−ligand interaction and others have also reported application of semiempirical QM methods to protein−ligand interaction.[22−24] Here, we report large-scale application of our QM-based method for binding affinity prediction. We validate our calculated binding affinities by comparing them to experimental binding free energies to measure the success of our method. We take a physically based approach wherein we account for all aspects of the binding phenomenon at various levels of approximation. Binding free energy in solution is calculated using the thermodynamic cycle shown in Figure 1. The electrostatic interactions between the ligand and the protein and between the solvent and the protein−ligand complex are treated at the highest levels of theory using semiempirical QM. Other interactions such as short-range and long-range nonpolar interactions are calculated using MM methods. We also dwell on different components of the scoring function and discuss their ability to predict binding free energy. In a related analysis we test the ability of the scoring function to discriminate between native and decoy binding modes or "poses".

Methods

Preparation of the Database. We compiled a database of 165 noncovalently bound protein−ligand complexes with an experimental binding affinity available in the literature.[25−35] This consisted of inhibition constants (K_i), dissociation constants (K_d), IC_{50} values, and calorimetric binding free energies. We converted all reported binding affinities to a free energy of binding reported in kcal/mol. All complexes along with their PDBIDs (PDB codes) and the binding free energies in this study are listed in Table SI of Supporting Information. In addition to preparing our own set we also exploited other publicly available sets.[28,36] For our validation studies we used the set prepared by Wang et al., which has 100 protein−ligand complexes.[28] This set is unique in its comparison of scoring functions available for docking. It compares the quality of binding affinity prediction for 11 available scoring functions that have been implemented in various commercial software packages such as SYBYL[37] and Cerius2.[38] However, after a careful visual inspection of the 100 available structures, we chose only 57 of the 100 protein−ligand complexes from this set.

We rejected protein−ligand complexes from this set based on the following criteria: (1) Metal-containing systems were excluded because metal atoms were not included in the scoring by Wang et. al., and hence, comparison with QMScore (which requires metal atoms to be included if they are in the active site) was not justified. (2) All the structures were visually compared with the original PDB entries, and if the ligand−inhibitor had missing functional groups, then it was excluded from the set. (3) In some cases there was ambiguity in the reported binding constants. For example, for tetrapeptide inhibitors bound to proteinase-A (PDB codes 4sga and 5sga), the Michaelis constant, K_M, was used as a measure of binding affinity for these inhibitors.[39] We excluded such complexes because we were interested only in thermodynamic constants such as K_d and K_i to calculate binding affinity from the structure and not the kinetic constants such as K_M. Using these criteria, we were left with 57 protein−ligand complexes from the set of 100.

Structure Preparation. Heteroatoms such as metals and ions not in the active site and water molecules were excluded from the PDB file. Protein and ligand atoms were extracted from each PDB file, and protons were added to all heavy atoms for the leap module of the AMBER 6.0 suite of programs.[40] Proton locations were assigned on the basis of standard geometries, and ionizable residues were protonated assuming physiological pH. The N and C termini were charged as in physiological pH conditions. For the small molecule, a combination of BABEL,[41] PRODRG,[42] and an in-house program was used to add protons to the heavy atoms in the ligands. The small molecule was then visually inspected, and if there was any conflict or ambiguity, then proton assignment was modified by hand. In the

case of Wang et al.'s data set, we visually inspected the preassigned protonation state of the ligand.

Atom Typing and Minimization. All protein and ligand atoms were assigned atom types for calculation of internal and nonbonded interaction energies and also for geometry optimization using a classical force field. The heavy atoms in the proteins were assigned atom types based on the AMBER 96 force field. For the ligand, the atom types were assigned with the Antechamber (which uses the generalized amber force field GAFF) module of the AMBER 7.0 suite of programs.[40] For geometry optimization of the protein−ligand complexes, we followed the following protocol. The heavy atoms were fixed at their experimentally observed positions by placing a high restraint of 5000 kcal mol^{-1} $Å^{-1}$, and geometries of the modeled protons were optimized using the AMBER 6.0 computer program. Five-hundred cycles of steepest decent were followed by 1000 cycles of conjugate gradient energy minimization. The complex was then taken apart, and hydrogen atom positions were reoptimized in the protein and ligand separately. However, X-ray crystal structures are far from being error-free and some of the structures have less than optimal geometric characteristics (e.g., unusually long or short bond lengths, close contacts, etc.).[43] Hence, in another protocol we performed full geometry optimization without any restraints on the heavy atoms. Five-hundred cycles of steepest decent was followed by 1000 cycles of conjugate gradient energy minimization. The protein and ligand were then taken apart and reoptimized separately using the same protocol. Quantum mechanics calculations were performed on the protein, the ligand, and the complex using both protocols.

Calculation of Binding Affnity. A thermodynamic cycle as shown in Figure 1 was used to calculate the free energy of binding of the ligand to the protein. This cycle can be summarized in the following set of equations:

$$\Delta G_{\text{bind}}^{\text{sol}} = \Delta G_{\text{b}}^{\text{g}} + \Delta G_{\text{solv}}^{\text{PL}} - \Delta G_{\text{solv}}^{\text{P}} - \Delta G_{\text{solv}}^{\text{L}}$$

$$\Delta G_{\text{b}}^{\text{g}} = \Delta H_{\text{b}}^{\text{g}} - T\Delta S_{\text{b}}^{\text{g}} \qquad (1)$$

The free energy of complex formation in solution was decomposed into gas-phase interaction energy $\Delta G_{\text{b}}^{\text{g}}$ and a solvation free energy $\Delta G_{\text{solv}}^{\text{PL}} - \Delta G_{\text{solv}}^{\text{P}} - \Delta G_{\text{solv}}^{\text{L}}$ of complexation. The gas-phase interaction energy is a sum of enthalpic and entropic contributions. The enthalpic contribution was calculated as a sum of electrostatic and nonpolar interaction energies. The gas-phase electrostatic interaction energy was calculated using our semiempirical divide and conquer (D&C) quantum mechanics program DivCon[14] at the AM1[15] or PM3[16] level of theory. DivCon calculates the heat of formation as

$$\Delta H_{\text{f}} = E_{\text{elec}} + E_{\text{core-core}} + \sum_{\text{atoms}} \Delta H_{\text{f}} \qquad (2)$$

where E_{elec} is the electronic energy and $E_{\text{core-core}}$ is the core−core repulsion calculated from the solute wave function. The sum over the heats of formation of all atoms in the system is added to the electronic energy and core−core repulsion to calculate the heat of formation of the system. The semiempirical quantum theory used to calculate the energy terms from the solute wave function[15,17,44] and details of the linear scaling technology[11−13] have been discussed in detail elsewhere. Briefly, the D&C approach involves division of a large biomolecule such as a protein−ligand complex into smaller subsystems and the electronic energy is obtained by solving a set of localized Roothaan−Hall equations,

$$\mathbf{F}^{\alpha}\mathbf{C}^{\alpha} = \mathbf{C}^{\alpha}\mathbf{E}^{\alpha} \qquad (3)$$

for each subsystem. Here, α is a subsystem, $\mathbf{F}^{\alpha}$ is the Fock matrix, $\mathbf{C}^{\alpha}$ contains the molecular orbital (MO) coefficients, and $\mathbf{E}^{\alpha}$ is the diagonal matrix of eigenvalues. The global Fock matrix **F** and the density matrix **P** are assembled from the subsystem matrices by variational minimization of the electronic energy using a self-consistent field (SCF) method. The electronic energy can subsequently be calculated as

$$E_{\text{elec}} = \frac{1}{2}\sum_{\mu=1}^{N}\sum_{\nu=1}^{N}(H_{\mu\nu} + F_{\mu\nu})P_{\mu\nu} \qquad (4)$$

where μ and ν are basis functions of the macromolecular system and **H** is the one-electron matrix.

For the protein−ligand interaction we calculated the heat of interaction (ΔH_{I}) between the protein and ligand as

$$\Delta H_{\text{I}} = \Delta H_{\text{f}}^{\text{PL}} - \Delta H_{\text{f}}^{\text{P}} - \Delta H_{\text{f}}^{\text{L}} \qquad (5)$$

where $\Delta H_{\text{f}}^{\text{PL}}$ is the heat of formation of the protein−ligand complex, $\Delta H_{\text{f}}^{\text{P}}$ is the heat of formation of the protein, and $\Delta H_{\text{f}}^{\text{L}}$ is the heat of formation of the ligand. We examined both the heat of formation and the electronic energy as representing the overall electrostatic energy of the system. This is further discussed in the Results and Discussion.

It is well-known that dispersive interactions are due to electron correlation that arise from favorable instantaneous multipole/induced multipole charge fluctuation.[45] These interactions are not captured by uncorrelated QM methods such as ab initio Hatree−Fock molecular orbital theory that describes each electron in the average field of the other electrons, or density functional theory (DFT) that uses local approximations for the density.[46,47] Often, large basis sets and higher levels of theory such as second-order perturbation (MP2) theory is invoked to describe dispersion interactions in molecular systems. However, these systems tend to be relatively small because of the prohibitive computational cost. Hence, to account for dispersion interactions in protein−ligand interaction, we used the attractive/dispersive ($1/R^6$) part of the classical Lennard-Jones interaction potential. This was calculated using the AMBER 96 force field[48] for nonbonded atoms in the protein−ligand complex. The enthalpic component of the gas-phase interaction energy was thus calculated as a sum of heat of interaction and the attractive part of the Lennard-Jones term.

Entropy plays an important role in binding. When protein and ligand form a complex, there is loss of 3 degrees of rotational and translational freedom, which makes it entropically unfavorable.[10,49,50] The entropic

contribution to binding can be described by a conformational and solvent component.[51] The number of rotatable bonds in the ligand has been a popular measure for conformational entropy used in a host of scoring functions.[25,52−54] In the process of binding the exposed amino acid side chains in the active site of the protein also lose conformational entropy when they are locked into a particular conformation via interactions with the ligand. The number of rotatable bonds in the protein side chains that interact with the ligand was added to the number of rotatable bonds present in the ligand. To enumerate the rotatable bonds in the protein, amino acid residues that were solvent-exposed in the unbound state but buried in the complex were tabulated. Then freely rotatable bonds were assigned on the basis of the number of rotamers of these amino acid residues. A conformational penalty of 1 kcal/mol was used for each rotatable bond.

The solvent entropy S_{sol} is the entropy gained by water molecules on being displaced from the active site by the ligand during binding. This can also be described as the hydrophobic effect in the context of binding. Structure-based thermodynamic calculations have shown the dependence of solvent entropy on the changes in solvent-exposed surface area during binding.[51] Other scoring functions such as ChemScore and DrugScore also use a surface area term to account for such effects.[54] We estimated solvent entropy based on the nonpolar and polar surface area burial during binding. A solvent probe radius of 1.4 Å was used to calculate the solvent accessible surface area (SASA).[55] The solvent entropy is calculated from the buried surface area as a result of complexation. Solvation free energy plays a very important role in binding.[50,52,56−58] From the perspective of binding it can be described as the desolvation of the ligand and the active site of the protein. The solvation free energy can be decomposed into electrostatic and nonpolar contributions. The electrostatic part of the solvation free energy was calculated using our self-consistent reaction field (SCRF) methodology, in which the polarization of the solute in the presence of a solvent reaction field is calculated with QM. The details of the method have been discussed elsewhere and have been recently reviewed as well.[59,60] Use of this method obviates an internal dielectric constant to calculate the solvation free energy because the QM solute polarization due to the solvent reaction field in effect describes the dielectric relaxation process.[59,61,62] By calculating the solvation free energy of the protein, ligand, and the complex, we evaluate the desolvation cost of the ligand and the protein active site during binding.

Molecular Recognition Model. In this study we also discuss the performance of the molecular recognition model (MRM), which is an intermolecular interaction based model for binding affinity prediction. The molecular recognition model has been previously described in the literature for understanding mechanisms of molecular recognition by computer simulations of protein−ligand interactions.[63] We adapted MRM with a few significant changes and implemented it in our computer program DivCon. The ligand−protein interaction energy was calculated as

$$E_{ij}^{inter} = E_{ij}^{dr} + E_{ij}^{es} + E_{ij}^{sol} \tag{6}$$

where E_{ij}^{inter} is the interaction energy between atoms i and j calculated as a sum of the dispersion−repulsion interaction energy E_{ij}^{dr}, the electrostatic interaction energy E_{ij}^{es}, and the pairwise solvation energy E_{ij}^{sol}. The dispersion−repulsion interaction was calculated using a soft-core 12-6 Lennard-Jones (LJ) potential as described by Verkhivker et. al., which is of the form

$$E_{LJ-soft} = \frac{A_{ij}}{(R_{ij}^{\ 6} + \delta_{LJ}^{\ 6})^2} - \frac{B_{ij}}{(R_{ij}^{\ 6} + \delta_{LJ}^{\ 6})^2} \tag{7}$$

where R_{ij} is the distance between atoms i and j and where the δ_{LJ} is the soft-core term for the LJ potential set at 2.75 Å. A_{ij} and B_{ij} were calculated using standard geometric combination rules. A reduced set of atom types were perceived from their geometry and connectivity within the molecule, and parameters were assigned automatically on the basis of the atom type by the computer program. The electrostatic interaction was calculated from a soft-core Columbic potential of the form

$$E_{ij}^{es} = \frac{q_i q_j}{4\pi\epsilon_0 D(R_{ij}^{\ 6} + \delta_{ES}^{\ 6})^{1/3}} \tag{8}$$

where q_i and q_j were solvated CM2 charges on atoms i and j calculated using an AM1 or PM3 Hamiltonian and the PB/SCRF method. The soft-core term δ_{ES} was set at 1.75 Å, and D was the dielectric constant set at 2.0. The pairwise solvation energy was calculated considering the transfer of an atom from the solvent to the active site of the protein. As described by Verkhivker et. al., the affinity of an atom for the solvent is proportional to the square of its partial atomic charge plus a constant:

$$S_i = \alpha q_i^{\ 2} + \beta \tag{9}$$

where S_i is the solvent affinity and q_i is the charge on atom i. α and β are constants set at $\alpha = 0.25$ kcal/mol and $\beta = -0.005$ kcal/mol. The volume of solvent displaced from atom i by atom j, X_j, is a function of the fragmental volume f_j of atom j and the distance of atom j from atom i. We also used a Gaussian weighting of the distance:

$$X_j = \frac{f_i \exp\left[-\frac{r_{eff}^{\ 2}}{2\sigma^2}\right]}{\sigma^3} \tag{10}$$

r_{eff} is the distance between the two atoms, which is used in the soft-core Coulombic term, and σ is a constant set at 3.5 Å. The solvation free energy in the protein−ligand interaction was thus calculated in a pairwise additive fashion using the expression

$$E_{ij}^{sol} = S_i X_j + S_j X_i \tag{11}$$

Regression Analysis. All the calculated terms were fit to experimental free energies of binding for the complexes in the data set using multiple linear regression (MLR). MLR seeks to minimize the error between

a dependent variable and independent variables using the ordinary least squares (OLS) method and has been used to compute weights or coefficients of various energy terms in scoring functions.[54,64−66] MLR thus allows us to assess the contribution of each of the independent variables to binding by calculating their weights and the predictive ability of the model by calculating the square of the correlation coefficient (R^2) and standard deviation. The following master equation was used to calculate binding free energy:

$$\Delta G_{\text{bind}} = \Delta H_{\text{I}} + \Delta \text{LJ}_6 + \Delta\Delta G_{\text{solv}} + \Delta S_{\text{solv}} + \Delta S_{\text{conf}} \quad (12)$$

The dependent variable or the experimental binding affinity (ΔG_{exp}) was fit to six independent variables, namely, ΔH_{I} (heat of interaction), ΔLJ_6 (the dispersive or $1/R^6$ part of Lennard-Jones interaction), $\Delta\Delta G_{\text{solv}}$ (solvation/desolvation free energy due to complexation), ΔS_{sol} (solvent entropy), and number of freely rotatable bonds (ΔS_{conf}). Similarly, for MRM the dispersion−repulsion interaction (E_{dr}), the electrostatic interaction (E_{elec}), and the solvation (E_{solv}) interaction between the ligand and the protein were fit to the experimental binding free energy. The coefficients estimated by the MLR were used to calculate the binding free energy (ΔG_{bind}) and square of the correlation coefficient (R^2). Henceforth, the score calculated for each protein−ligand complex from regression analysis is referred to as QMScore. We note that in our previous work we have described the TotalScore for predicting binding affinity.[22] To make the distinction clear again, TotalScore is simply the raw sum of the individual contributions used in eq 12 without any of the weights calculated by linear or nonlinear methods. However, when comparing QMScore and TotalScore we fit TotalScore to experimental binding free energy.

Predicting Binding Mode. We used the set prepared by Wang et al. for testing our method's ability to discriminate between native and decoy binding modes. This set comprises 100 protein−ligand complexes spanning different protein families. For each of the protein−ligand complex, Wang et. al. generated 100 decoy poses using AUTODOCK. We obtained these poses and scores for all 100 protein−ligand complexes. From this set we chose 20 protein−ligand complexes and 50 decoy poses for each target to test our scoring function. These 20 protein−ligand complexes are listed in Table 2. The native pose decoy complexes were prepared by performing geometry optimization on the added hydrogen atom positions as described in the protocol above. The native poses and the decoy poses were scored using TotalScore, and the results were then analyzed.

Calculating Proton Affinity. The inhibitors that bind to HIV-1 protease are known to have either one or two hydroxyl groups. We have used our calculations to assign the protonation states of the aspartyl dyad in the presence of the inhibitors of HIV-1 protease. Four protonation states were considered where the proton was bonded to either OD1 or OD2 oxygen of the catalytic aspartates ASP25 and ASP25′. For protonation state A, the OD2 oxygen of ASP 25 was protonated, and for state B, the OD1 oxygen of ASP 25 was protonated. Similarly, for protonation state C, the OD2 oxygen of ASP 25′ was protonated, and for protonation state D, the OD1 oxygen of ASP 25′ was protonated (Table SIV in Supporting Information). The proton affinity for each of the dyads in 26 complexes was calculated as follows:

$$\text{proton affnity (PA)} = \Delta E_{\text{PL−H}} - \Delta E_{\text{PL}} \quad (13)$$

where

$$\Delta E = \Delta H_{\text{P}} + \Delta \text{LJ}_6 + \Delta\Delta G_{\text{solv}} \quad (14)$$

PL-H is the protonated form and PL is the unprotonated form of the protein−ligand complex. ΔH_{P} is the heat of protonation/deprotonation, ΔLJ_6 is the dispersive energy due to protonation/deprotonation, and $\Delta\Delta G_{\text{solv}}$ is the solvation cost of protonation/deprotonation. All these terms were calculated in the presence of the ligand. The gas-phase heat of protonation (ΔH_{P}) was calculated at the AM1 level of semiempirical theory, and solvation correction was applied using our PB/SCRF method with a CM2 charge model. The nonpolar interaction energy was estimated from the dispersive part of the Lennard-Jones interaction using AMBER 96 force field. In Table SIV of Supporting Information, we have listed the proton affinity of the aspartates 25 and 25′ in the presence of the inhibitor for 26 inhibitors bound to HIV protease. The individual contributions to proton affinity have not been listed in the table, but the differences in proton affinity arise from the electrostatic and solvation components of the interaction energy and not from the dispersive/attractive interaction energy.

Results and Discussion

Binding Affinity Prediction. For predicting binding affinity we used a diverse set of 165 complexes containing different protein families including aspartic proteases, serine proteases, sugar binding proteins, amino acid binding proteins, and protein kinases. Figure 2 shows calculated ΔG_{bind} versus experimental ΔG_{bind} for the 165 complexes. This scoring function is able to capture the general trend with respect to variation in binding affinity for a diverse set of protein−ligand complexes from the PDB. The square of the correlation coefficient between the TotalScore (TotalScore is the sum of all parts of the scoring function; see Methods) and the calculated binding affinity is 0.48 with a standard deviation of 2.11 kcal/mol. By using MLR to fit different parts of TotalScore (yielding QMScore), we obtained the square of the correlation coefficient R^2 between calculated and experimental ΔG_{bind} of 0.55. The standard deviation between the calculated and experimental ΔG_{bind} was 1.98 kcal/mol.

Since the X-ray crystal structures used had a wide range of resolution, we also studied the relationship between the quality of prediction and the resolution, internal energy of bonds, angles, and nonbonded repulsive interactions calculated using the AMBER force field. We find that the quality of prediction (R^2) has a well-defined relationship with bond energy, angle energy, and the repulsive part of the nonbonded interactions (which represents steric clashes in the structure). The R^2 between TotalScore and experimental ΔG_{bind} decreases with an increase in bond energy and angle energy that represent deviations from standard bond lengths and angles in the crystal structure (Figure 3). Similar results were obtained for the repulsive part of the nonbonded interaction (data not shown). These

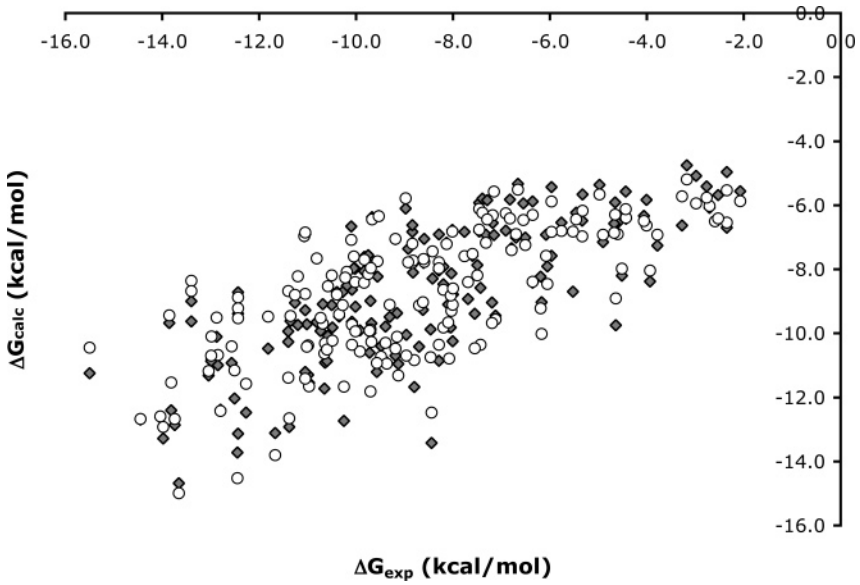

Figure 2. Calculated vs experimental ΔG of binding for 165 protein−ligand complexes from the PDB. (◆) Data points are calculated without fitting components of the score to experimental ΔG of binding ($R^2 = 0.49$). (○) Data points are calculated by fitting components of the score to experimental ΔG of binding ($R^2 = 0.55$).

results imply that the scoring function is very sensitive to geometries and its predictive ability depends on the quality of the structures used. In this regard our scoring function is different from other empirical or knowledge-based potentials because these potentials are not necessarily penalized by structures of poorer quality.

Our data set consisted of diverse protein targets and families, and we assessed the performance of our scoring function within these protein families. For a set of 29 HIV-1 protease complexes, we obtained a square of the correlation coefficient R^2 of 0.24. The R^2 increases to 0.32 without one outlier (TotalScore in Table 1a). When different contributions to TotalScore is fit to the experimental ΔG_{bind} (QMScore in Table 1a), the R^2 for the set is 0.36 with one outlier and is 0.43 without one outlier. The standard deviation between experimental and calculated ΔG_{bind} is 1.51 kcal/mol for this set and 1.38 kcal/mol without one outlier. HIV-1 proteases are enzymes that recognize peptides and are capable of cleaving peptide bonds with sequence selectivity.[67] The enzyme binding sites are complementary to substrate residues. The free energy of binding between these proteases and their natural substrates have a significant entropic component because the substrates are peptides and have conformational degrees of freedom that are lost because of binding. Estimation of this part of the free energy is based on an empirical count of rotatable bonds and is a poorly estimated quantity in our scoring scheme that affects this set. Also, the active site in the apo protein is thought to be more open because of the large-scale motion of the "flap" regions in the protease not taken into consideration in this approach.[68] These approximations could explain the modest R^2 values for this set. Indeed, other scoring functions such as the knowledge-based potential (KBP) SMOG[53] had poor agreement with experimental binding affinities for aspartic proteases ($R^2 = 0.03$ for SMOG96 and $R^2 = 0.38$ for SMOG2001) compared to other protein families. Another KBP PMFScore was used by Muegge and Martin[69] to calculate binding affinity not from X-ray crystal structures but from inhibitor poses minimized in the active site of the crystal structure of L-689,502 inhibited HIV-1 protease taken from Holloway and coworkers.[70] The empirical scoring function VALIDATE performed better on aspartic proteases ($R^2 = 0.74$), but it fit 29 variables or descriptors to the experimental binding affinity.[65] Overall, the HIV-1 protease set, while very well characterized structurally, still poses a significant challenge to modeling its binding affinity.

The catalytic dyad of aspartic acid residues in aspartic proteases plays a crucial role in peptide hydrolysis using a general acid catalysis mechanism. It has been concluded that one of the aspartates is protonated while the other is unprotonated for the enzyme to be catalytically competent.[67] The proton titration behavior of the aspartyl dyads have been studied experimentally and shown to yield two distinct pK_a values.[71] Since the two aspartyl groups are chemically equivalent, it is not possible to associate the pK_a value with a particular aspartate residue in the enzyme. Atomic resolution information from X-ray crystallography cannot resolve the hydrogen positions at low resolution. Recently a method for computational titration of HIV-1 protease has been reported[72] and our linear scaling QM method has also been used by Rajamani and Reynolds to model the protonation state of catalytic aspartates in β-secretase (BACE).[73]

We calculated proton affinity in all four possible protonation states for 26 inhibitors bound to HIV-1 protease (see Methods and Table SIV of Supporting Information). The general trends for proton affinity in the ligands agree with hydrogen-bonding patterns between the inhibitors and the enzyme. For inhibitors with a single hydroxyl group interacting with the catalytic dyad such as A76889, A78791, AQ148, GR126045, hydroxyethylene, L-700417, SB203386, and SB206343, the protonation state with an optimal hydrogen bond distance between the heavy atoms (2.8−3.2Å) has the greatest proton affinity. For inhibitors with two hydroxyl groups (diols) the results are less intuitive. However, for inhibitors such as DMP323, DMP450, SD146, A77003, and XK263, proton affinity is greatest

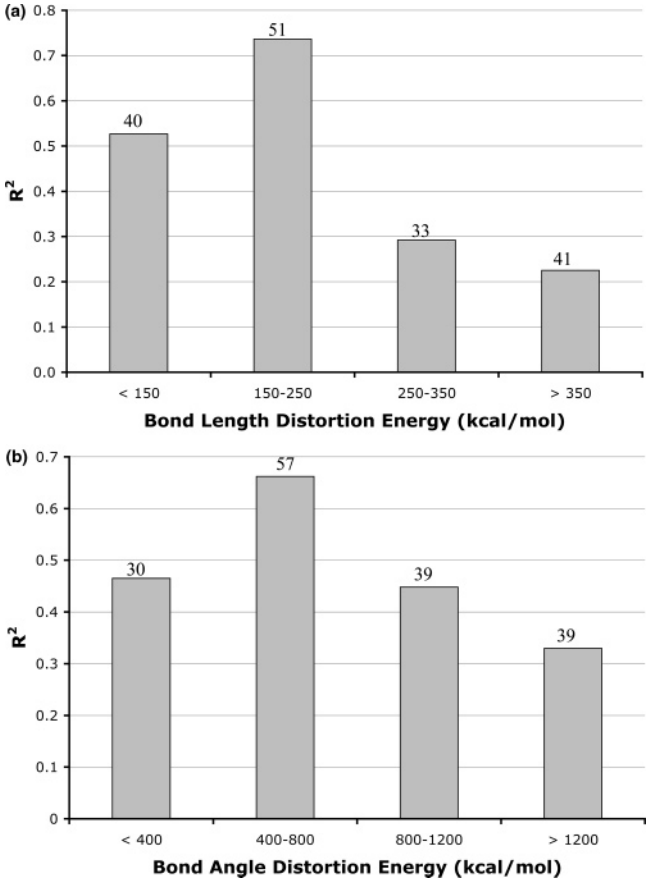

Figure 3. (a) Dependence of the square of the correlation coefficient R^2 (ΔG_{calc} vs ΔG_{expt}) on bond length distortion energy. The number of protein−ligand complexes in each bin is labeled on the bars. (b) Dependence of the square of the correlation coefficient R^2 (ΔG_{calc} vs ΔG_{expt}) on bond angle distortion energy.

for the state with at least one optimal hydrogen-bonding interaction. These calculations in some cases also show a distinct preference for one aspartate over the other in the catalytic dyad. This is evident for inhibitors such as A74704, A76889, AQ148, DMP323, GR126045, L-700417, and U75875. If acidic residues in other proteins have distinct pK_a values implying the presence of a titratable proton on either of the residues, then one can ascertain the protonation state by using this method. Inhibitors designed with a more accurate protonation state are likely to be more effective.

Choosing the protonation state accurately can also lead to a better performance of scoring functions. In a test of this notion, we chose the receptor protonation state with the greatest proton affinity for calculating the binding free energy between 26 inhibitors with a hydroxyl or diol group interacting with the catalytic aspartate dyad of HIV-1 protease. For three complexes in which inhibitors did not have a hydroxyl group or diol group present, we calculated the interaction, ignoring the protonation state as done previously. TotalScore and QMScore were calculated by fitting various contributions to the experimental binding affinity. It was found that, barring VX478, the binding affinity calculated using the QMScore in the latter manner gave a better agreement with experimental binding affinities. We obtained an R^2 of 0.29 for TotalScore and 0.46 for QMScore when different contributions were fit to experimental data. The standard deviation in this case was 1.31 kcal/mol, which was lower than the 1.51 kcal/mol for the set in which the protonation states were ignored in QMScore calculations.

For the serine protease family we obtain good correlation with experimental ΔG_{bind}. The serine protease set had 19 protein−ligand complexes from the PDB that included thrombin and trypsin inhibitors. For this set we obtained a R^2 of 0.69 for TotalScore. For QMScore, we obtain an R^2 of 0.78 and a standard deviation of 1.5 kcal/mol (Table 1a). Without one outlier we obtain R^2 of 0.69 and 0.8 for TotalScore and QMScore, respectively, and a standard deviation of 1.38 kcal/mol. For this set we perform comparably to other scoring functions in the literature.[26,74] For 11 protein kinase inhibitors we achieve an R^2 value of 0.47 and 0.67 for TotalScore and QMScore, respectively. Without one outlier the R^2 increases to 0.58 and 0.95 for TotalScore and QMScore with a standard deviation of 0.37 kcal/mol. The dramatic increase in R^2 without one outlier for QMScore is due to overfitting because the number of observations is not large compared to the number of independent variables in the QMScore master equation.

For 40 metalloenzyme complexes we obtain good agreement with the experimental ΔG_{bind} with an R^2 of 0.55 and 0.58 for TotalScore and QMScore, respectively. The standard deviation for this set is 1.67 kcal/mol. Without one outlier, however, TotalScore and QMScore have R^2 of 0.68 and 0.7, respectively, with a standard deviation of 1.43 kcal/mol. This set includes human carbonic anhydrase, carboxypeptidase, and matrix metalloproteases inhibitors and highlights the strength of our scoring function and its ability to capture the binding free energy variations in metal-containing protein−ligand systems. This is unique to our scoring function because other empirical, KBPs, and force field based methods tend to ignore the interaction of the metal with its environment even though significant electrostatic effects between the ligand and the metal are likely. QMScore's performance in predicting binding affinity for different protein families has been tabulated in Table 1a. We achieve good agreement in all cases with an average standard deviation between calculated and experimental ΔG_{bind} of less than 2.0 kcal/mol.

This is an encouraging result because we are computing binding free energies of protein−ligand complexes from a single X-ray crystallographic structure in which only the positions of the protons have been optimized using a force field. We assume that the X-ray crystal structure of the ligand is the global minimum energy conformation and is conformationally and energetically distant from the nearest maximum on the binding free energy surface. However, it is quite possible that the affinity of a ligand for a protein target depends on an ensemble of conformationally close ligand poses that contribute to the free energy of binding.[75] To assess the dependence of the interaction energy on the conformation of the ligand, we have calculated the ΔH_I, dispersion interaction, and solvation free energy of poses close to the X-ray crystal structure.

In Table 1b we have listed the average gas-phase interaction energy (ΔH_I), the dispersive part of the Lennard-Jones interaction, and the solvation free energy ($\Delta\Delta G_{solv}$) for five protein−ligand complexes with

Table 1.

(a) Performance of QMScore within Protein Families Based on X-ray Crystal Structures[a]

protein family	no. of complexes	R^2 TotalScore	R^2 QMScore	SD (kcal/mol)	ΔG_{bind} range (kcal/mol)
HIV-1 protease	29	0.24	0.36	1.51	6.7
HIV-1 protease without 1 outlier	28	0.32	0.43	1.38	6.7
HIV-1 protease (best PA)[b]	29	0.29	0.46	1.31	6.7
serine protease	20	0.69	0.78	1.50	10
serine protease without 1 outlier	19	0.69	0.80	1.38	10
protein kinase	11	0.47	0.67	1.07	5
protein kinase without 1 outlier	10	0.58	0.95	0.37	5
metalloproteins	40	0.55	0.58	1.67	14
metalloproteins without 1 outlier	39	0.68	0.70	1.43	14

(b) Distribution of the Average Interaction Energy and Its Contributions for Native and Near-Native Poses for Five Protein−Ligand Complexes Spanning 10 kcal/mol of Binding Free Energy[c]

protein−ligand complex	ΔG_{bind} (kcal/mol)	av rmsd (Å)	av ΔH_I (kcal/mol)	av ΔLJ_6 (kcal/mol)	av $\Delta\Delta G_{solv}$ (kcal/mol)
trypsin benzamidine	−2.51	0.60	−163.22	−51.70	179.83
		(0.46)	(8.03)	(3.81)	(3.10)
plasminogen kringle-aminocaproic acid	−5.97	1.64	−126.57	−46.10	165.68
		(1.22)	(16.38)	(4.82)	(11.85)
56Lck Sh2 domain−inhibitor	−6.05	2.38	−321.83	−124.46	424.78
		(1.83)	(26.69)	(21.52)	(22.25)
DHFR−folate	−10.28	1.43	−286.41	−113.14	310.80
		(1.06)	(76.82)	(7.50)	(6.20)
penicillopepsin−pepstatin analogue	−12.98	2.38	−479.21	−138.53	553.07
		(1.93)	(26.19)	(17.59)	(7.07)

[a] For TotalScore, individual contributions have not been fit to experimental ΔG_{bind}. For QMScore, individual contributions have been fit to experimental ΔG_{bind}. SD is the standard deviation of the calculated from the experimental ΔG_{bind}. [b] ΔH_I, ΔLJ_6. $\Delta\Delta G_{solv}$ is used for complexes with the best proton affinity (PA). See Results and Discussion. [c] The standard deviation is in parentheses.

four poses closest to the X-ray crystal structure pose. The poses were generated using AUTODOCK by Wang et. al. and chosen on the basis of root-mean-squared deviation (rmsd) from the native. The trends in Table 1b underline the challenges in the prediction of binding free energy using physically based energy functions. The standard deviation for ΔH_I for all complexes is in the tens of kcal/mol, whereas the standard deviation for $\Delta\Delta G_{solv}$ is generally lower in magnitude. The sensitivity of these interaction energies to ligand geometries is also demonstrated in the table. Even for a tighter distribution of near-native structures such as the trypsin−benzamidine complex (average rmsd of 0.6; standard deviation (SD) of 0.46), the variation in calculation of ΔH_I is ∼8 kcal/mol. For a more relaxed distribution of binding modes, such as in the penicillopepsin−pepstatin analogue complex (av rmsd of 2.38; SD of 1.93), the variation in calculation of ΔH_I is as high as 26 kcal/mol. The magnitude of the variation in estimation of different quantities is much greater than the range of experimental binding free energy. Despite these challenges, this first-generation scoring function can predict binding free energy trends in protein−ligand interaction with reasonable accuracy.

Binding Affinity Prediction from Docked Poses. In the absence of atomic structures determined by either X-ray crystallography or NMR, QMScore can be used to determine the binding affinity from ligand poses docked to protein targets. The poses can be obtained using any one of the standard docking programs (e.g., DOCK,[76] Autodock,[77] ICM,[78] etc.). We demonstrate this by calculating the QMScore for two sets of protein−ligand complexes. The first set consisted of inhibitors that were modeled and minimized by Holloway et al., in the active site of the HIV-1 protease bound to the inhibitor L-689,502 using the Merck molecular mechanics force field (MMFF).[79] The catalytic water 407 in the "flap" region of the protease was included in the minimization of the inhibitors in the active site of the protease.[70] We obtained the coordinates of the protease and the inhibitors from the authors and performed QMScore calculations. The pK_i was calculated using the QMScore scoring model by fitting the individual components to the experimental pK_i. For the 33 complexes we achieve good correlation with the experimental pK_i with an R^2 of 0.58. The standard deviation between calculated and experimental pK_i is 0.94 pK_i units. Without one outlier, the R^2 increases 0.63 with an average standard deviation of 0.88 pK_i units. Although the overall R^2 for the 33 inhibitors was modest, the standard deviation was less than 1 pK_i. Moreover, these poses have been minimized in the active site using MMFF and are not X-ray crystal structures.

In another set we used QMScore to calculate pIC_{50} values for a set of 60 inhibitors docked to the matrix metalloprotease stromelysin (MMP-3). The poses were docked by Jacobbson et. al. into the active site of MMP3 (PDB code: 1HY7) using ICM. The authors also scored the poses with ICM and PMF.[36] We calculated the pIC_{50} values of these inhibitors using our QMScore model for this set of 60 docked inhibitors and obtained an R^2 of 0.6 (Figure 4b). The standard deviation of prediction for this set was 0.47 pIC_{50} units. In Figure 5 we show the diversity of this set of 60 inhibitors and list the experimental and calculated pIC_{50} values. The range of pIC_{50} values for this set of diverse MMP-3 inhibitors is ∼3 pIC_{50} units, which makes this result quite significant because it highlights the resolution of the method. Jacobbson et. al. have scored these complexes with PMF and a showed a weak correlation with an R^2 of 0.27,

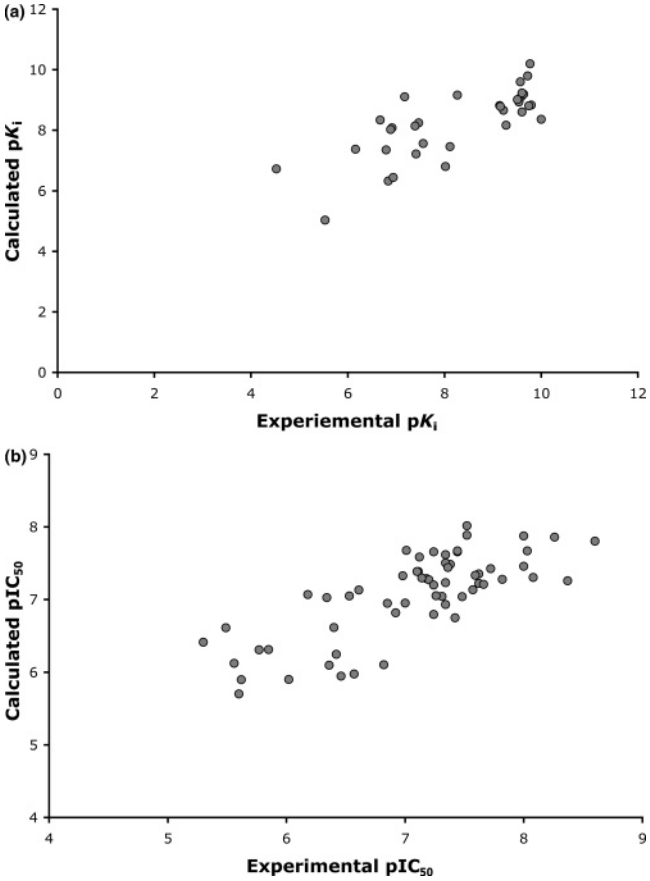

Figure 4. (a) Calculated versus experimental pK_i for 33 inhibitors minimized in the active site of the crystal structure of L-689,502 inhibited HIV-1 protease. Coordinates of the protein and the inhibitors are provided by Holloway.[70] The square of the correlation coefficient is 0.58 with a standard deviation of 0.94 pK_i units. (b) Calculated pIC$_{50}$ versus experimental pIC$_{50}$ for 60 inhibitors docked to matrix metalloprotease 3 protein (PDB code 1hy7). The square of the correlation coefficient (R^2) is 0.6 with a standard deviation of 0.47 pIC$_{50}$ units.

while ICM had no correlation with experimental pIC$_{50}$ values. These results suggest that QMScore can be used to calculate binding affinity with a standard deviation of less than one binding affinity unit even when the X-ray structures of the ligand−protein complexes are not available. Such a prediction model can be used to search for leads in a database or for lead optimization stages of any high-throughput docking experiment.

Comparison with Other Scoring Functions. We also compared the performance of QMScore with other scoring functions available in the literature. We used the data compiled by Wang et al. for the assessment of empirical and knowledge-based scoring functions.[28] They have compared scoring functions for 100 protein−ligand complexes from the PDB. However, out of the 100 complexes, only 57 were suitable for scoring and comparison with the performance for the 11 scoring functions (see database preparation section in Methods). We compared the performance of QMScore with other scoring functions for this set of 57 protein−ligand complexes. Figure 6 shows the correlation between experimental ΔG_{bind} and QMScore. TotalScore has not been fit to the experimental binding free energies and correlates with binding affinity with an R^2 of 0.48. When different components are fit to the experimental ΔG_{bind}, the R^2 is 0.53 (QMScore). In Figure 6 we have compared the R^2 for different empirical and knowledge-based scoring functions, and QMScore outperforms all other scoring functions for this set. LigScore, GScore, and DrugScore are second to QMScore with lower R^2 values ($R^2 = 0.45$). Interestingly, DrugScore is a knowledge-based potential, while GScore is an empirical potential that has been fit to discriminate between native and decoy binding modes.

Electronic Interaction Energy and Binding Free Energy. In our calculations we used the heat of interaction to model the electrostatic interaction between the protein and ligand, and while the heat of interaction is a more physically based description of the interaction, we find that the electronic part of interaction correlates highly with experimental ΔG_{bind}. In Figure 7a we have plotted the electronic interaction energy (in keV) with the experimental binding free energy for 16 serine protease inhibitors. The R^2 between the electronic interaction energy and the experimental ΔG_{bind} is 0.88. There is one outlier, and if it is removed, the R^2 increases to 0.92. The R^2 for QMScore for the same set is 0.77 (Table 1). For 60 MMP inhibitors docked in the active site of MMP-3, the electronic interaction energy correlates with experiment with an R^2 of 0.57 and 0.66 without one outlier (Figure 7b). R^2 for the QMScore model for the same set is 0.6 as reported in the previous section. It is encouraging to find that the electronic interaction energy by itself is able to determine binding trends with reasonable accuracy. Finally, for the set of 57 protein−ligand complexes from Wang et al.'s set, the electronic interaction energy correlates with binding affinity with an R^2 of 0.46 (Figure 6).

Since the electronic interaction energy is not fit to any empirical observations, we see it as a physically based score that can be used to understand the effect of different preparatory schemes and methods on binding free energy prediction. For example, we tested the effect of geometry optimization of the entire protein−ligand complex using the AMBER molecular mechanics force field on the prediction of binding affinity. Interestingly, optimization of the protein−ligand geometry with the AMBER force field marginally improved the agreement with the experimental ΔG_{bind}. This only marginal improvement (R^2 of 0.462 for AM1 and 0.463 for PM3) emphasizes the importance of experimental geometries for the protein−ligand complex and the limitation of GAFF to describe the geometry of the ligand and its interactions with the protein. Indeed, in related data sets where different ligands were bound to one protein target, electronic interaction energy is as good a descriptor of the binding free energy as the more detailed QMScore model that takes into account all contributions toward binding. Since the electronic interaction energy is not fit to any experimental information, we believe this score reflects electrostatic interactions between the ligand and the protein in the active site. Regardless, using the interaction energy exclusively ignores important effects such as solvation and conformational entropy and, hence, is likely to fail in cases where this is important.

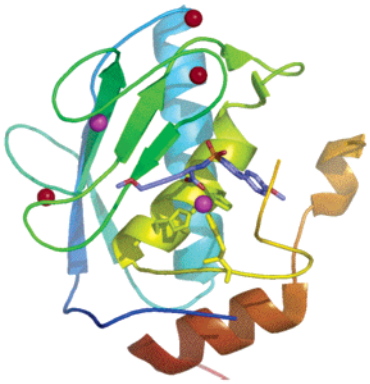

Compound No.	Structure	Experimental pIC_{50}	Calculated pIC_{50}
1	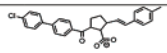	5.3	6.41
2	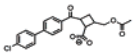	5.49	6.61
3	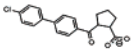	5.56	6.12
4	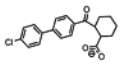	5.6	5.7
5	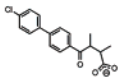	5.62	5.9
6	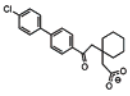	5.77	6.31
7	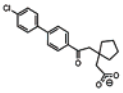	5.85	6.31
8	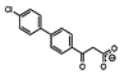	6.02	5.9
9	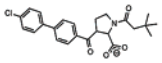	6.18	7.07
10	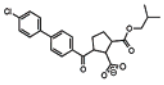	6.34	7.03
11	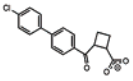	6.36	6.10
12	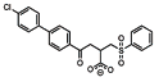	6.4	6.62
13	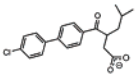	6.42	6.25
14	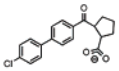	6.46	5.95
15	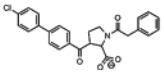	6.53	7.05

Compound No.	Structure	Experimental pIC_{50}	Calculated pIC_{50}
16	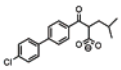	6.57	5.98
17	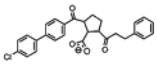	6.61	7.13
18	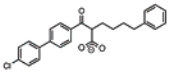	6.82	6.1
19	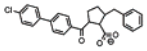	6.85	6.95
20	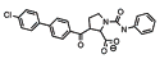	6.92	6.82
21	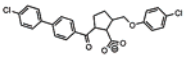	6.98	7.33
22	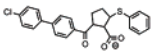	7.0	6.95
23	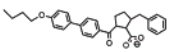	7.01	7.68
24	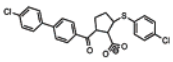	7.1	7.34
25	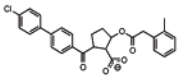	7.11	7.39
26	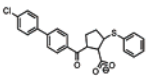	7.12	7.59
27	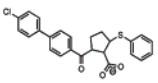	7.14	7.3
28	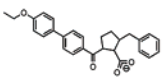	7.18	7.29
29	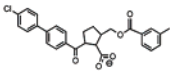	7.2	7.27
30	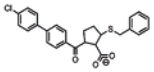	7.24	6.8
31	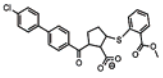	7.24	7.20

Figure 5. (Continued on next page)

Compound No.	Structure	Experimental pIC_{50}	Calculated pIC_{50}
32	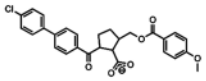	7.24	7.66
33	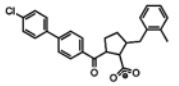	7.26	7.05
34	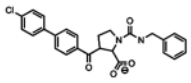	7.31	7.04
35	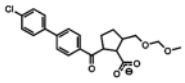	7.34	6.93
36	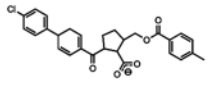	7.34	7.23
37	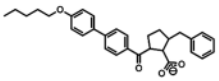	7.34	7.62
38	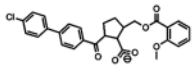	7.34	7.5
39	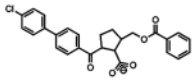	7.36	7.44
40	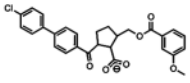	7.38	7.49
41	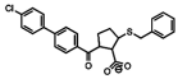	7.42	6.75
42	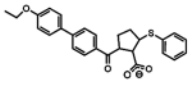	7.44	7.66
43	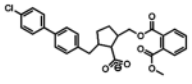	7.44	7.67
44	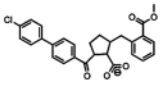	7.48	7.04
45	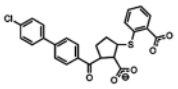	7.52	7.89
46	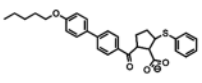	7.52	8.02
47	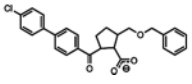	7.57	7.13
48	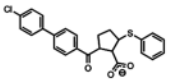	7.59	7.33
49	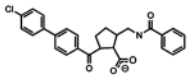	7.62	7.35
50	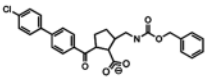	7.62	7.22
51	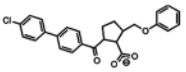	7.66	7.2
52	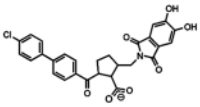	7.72	7.4
53	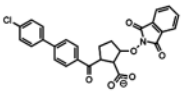	7.82	7.2
54	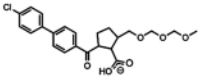	8.0	7.4
55	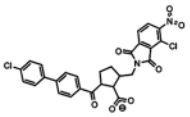	8.0	7.8
56	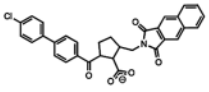	8.03	7.6
57	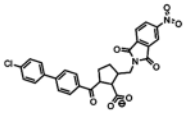	8.08	7.3
58	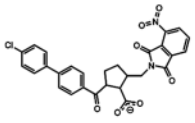	8.26	7.8
59	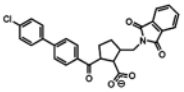	8.37	7.2
60	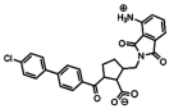	8.6	7.8

Figure 5. Ribbon diagram of matrix metalloprotease 3 (MMP3) stromelysin (PDB code 1HY7) with bound ligand (purple). The histadine residues coordinating the zinc atom are shown in yellow. Zinc atoms are colored magenta, and calcium atoms are colored red. Experimental and calculated pIC_{50} for 60 inhibitors docked in the active site of MMP3 with the docking program ICM. Data are from Jacobsson et al.[36]

Molecular Recognition Model. We have used the molecular recognition model (MRM) with reduced AMBER atomtypes and CM2 charges to design a scoring function for binding free energy prediction that takes into account only the intermolecular interactions between the protein and the ligand (see Methods). Polarization and charge-transfer effects are captured in the atomic point charges derived from the solute electron density. The main feature of MRM is the softened interaction potential and atom-based solvation that makes it pairwise additive in nature and easy to implement. Softened potentials have been shown in docking simulations to smooth out the binding free energy surface, to enhance sampling, and to identify

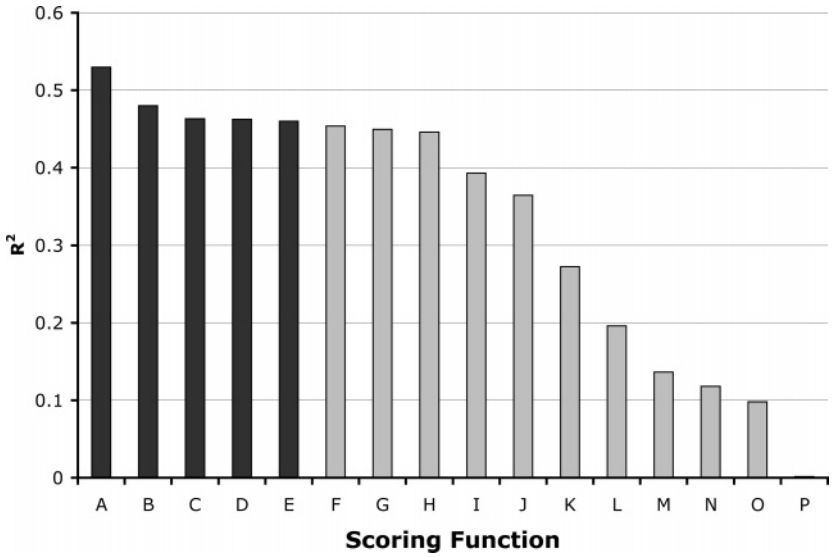

Figure 6. Comparison of QMScore with other scoring functions for predicting binding affinity for a set of 56 protein−ligand complexes from Wang et al.'s data set. The letters correspond to the following: (A) QMScore; (B) TotalScore; (C) PM3 electronic interaction energy for geometry optimized PL complexes; (D) AM1 electronic interaction energy for geometry optimized PL complexes; (E) AM1 electronic interaction energy for only hydrogen geometry optimized PL complexes; (F) LigScore; (G) Gscore; (H) DrugScore; (I) PMF; (J) Xscore; (K) PLP; (L) Dscore; (M) LUDI; (N) ChemScore; (O) Fscore; (P) Autodock.

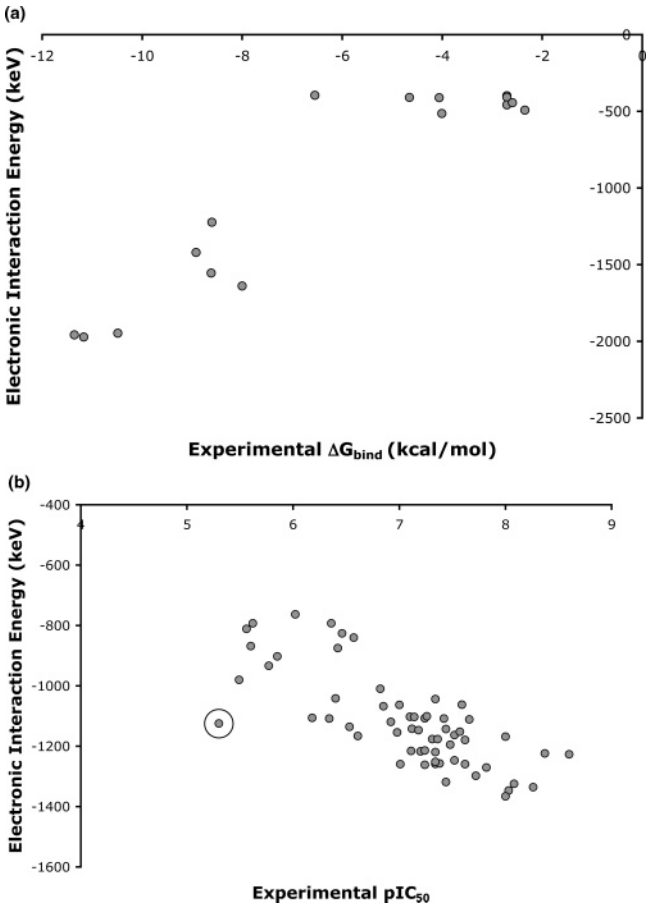

Figure 7. (a) Electronic interaction energy versus experimental ΔG_{bind} for a set of 16 serine protease inhibitors. R^2 for this set is 0.88. (b) Electronic interaction energy versus experimental pIC_{50} for a set of 60 inhibitors docked to MMP3 (PDB code 1hy7). R^2 for this set without one outlier (in circle) is 0.66.

known ligands in virtual screening.[63,80] We find this softened potential to reliably predict experimental binding affinity within the set of HIV-1 protease inhibitors

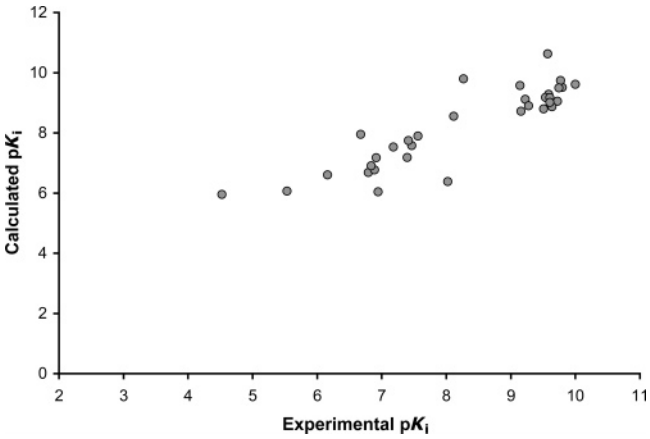

Figure 8. Performance of the molecular recognition model for a set of 33 inhibitors minimized in the active site of HIV-1 protease. The R^2 for this set is 0.78 with an SD of 0.65 pK_i units between experimental and calculated pK_i.

that we tested. This set comprised 33 inhibitors minimized in the active site of HIV-1 protease[70] that were also scored with QMScore, as described above. The catalytic water molecule (water 407) seen in the X-ray crystal structure was considered as a part of the ligand, and these inhibitors were scored using MRM with solvated CM2 charges calculated using the AM1 Hamiltonian. We fit the dispersion−repulsion, electrostatic, and solvation components of MRM to the experimental pK_i and obtain an R^2 of 0.78 and an rmsd of 0.67 pK_i units (Figure 8). The R^2 for MRM scores without fitting components to the experimental pK_i values is 0.72. This is a very good agreement considering that MRM is essentially a molecular mechanics based scoring scheme that only calculates intermolecular interactions between the ligand and the protein.

To assess the impact of polarization and charge-transfer effects on calculated pK_i, we used fixed AMBER point charges for the protein atoms in all 33 protein−ligand complexes. CM2 charges were used for the ligand and the catalytic water 407, calculated using the AM1

Hamiltonian. We find that the total MRM score that is not fit to the experimental pK_i values in this case is 0.69, which is slightly lower than the R^2 of 0.72 when polarization and charge transfer is included in the CM2 charges. However, when different components are fit to the experimental pK_i values, the R^2 is 0.81 with an SD of 0.63 kcal/mol. The decrease in R^2 for MRM-total in the second case highlights the importance of the polarization and charge transfer in protein−ligand interactions; however, at least in this case there is only a modest decrease in the agreement with experimental pK_i values. Moreover, the deficiency of using a fixed charge model can apparently be overcome by using MLR to fit the components of MRM to experimental pK_i values. Although fitting to experimental data leads to the dependence of coefficients or weights on the experimental data set, there is always an issue of transferability of the coefficients derived using MLR for new situations.

Discussion of soft-core potentials is incomplete without addressing the dependence of the quality of agreement between the MRM scores and experimental pK_i values on the soft-core constant. In Figure S1 of the Supporting Information, the square of the correlation coefficient between experimental pK_i values and raw MRM (MRM-total) scores, and experimental pK_i values and MRM-fit scores, against the soft-core constants both for the dispersion−repulsion interaction (δ_{DR}) and for the electrostatic interaction (δ_{ES}) is plotted. Starting with a δ_{ES} of 1.75 Å, the value of δ_{DR} was scanned in order to locate the value where the agreement between the calculated pK_i and the experimental pK_i was the best.

For MRM-total, the best agreement between experimental pK_i values and MRM-total (R^2 maxima) is at a value of 1.9Å for δ_{DR}, whereas for MRM-fit the R^2 maxima spans a range of 1.0−1.5Å for δ_{DR}. Using a value of 1.9 Å for δ_{DR}, δ_{ES} was scanned for the best agreement between calculated and experimental pK_i values. It was found that the best agreement corresponds to a value of 1.65 Å for δ_{ES}. Therefore, softening potentials impact binding free energy prediction. Softening potentials also implicitly account for receptor and ligand flexibility and have been used successfully in protein−protein[81] and protein−ligand docking.[82] It is quite possible to tune soft-core constants for different protein targets in order to maximize accuracy of prediction.

Discriminating Native from Decoys. The performance of any scoring function can be assessed by its ability to predict the binding affinity when the experimental binding mode is available. However, docking programs also use scoring functions to predict the binding modes of ligands for which atomic information obtained through X-ray crystallography or nuclear magnetic resonance is unavailable. A scoring function that can accurately predict the binding affinity as well as the binding mode is highly desirable in structure-based drug design. The ability of any scoring function to predict binding modes is tested by whether it can discriminate between the native binding mode obtained from either X-ray crystallography (as in this study) or NMR and from "decoy poses" generated by the in silico sampling of conformational space.

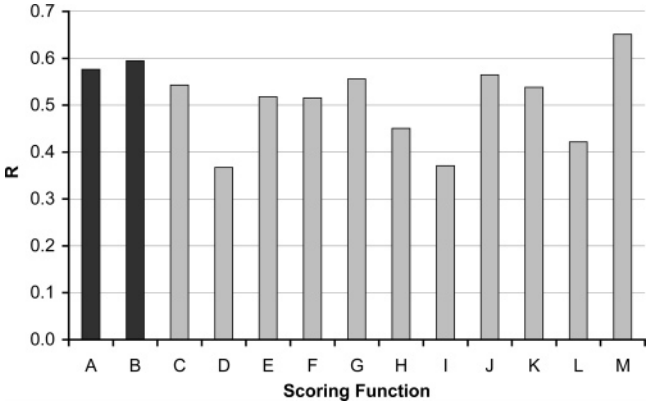

Figure 9. Comparison of QMScore with other scoring functions for ability to discriminate between native and decoy poses for 50 protein−ligand complexes. R is correlation coefficient between score and rmsd of the pose from the native binding mode. The letters correspond to the following: (A) TotalScore1 is the sum of all contributions; (B) TotalScore2 has electrostatic interaction weighted twice as much as other contributions; (C) Autodock; (D) ChemScore; (E) DrugScore; (F) Dscore; (G) Fscore; (H) Gscore; (I) LigScore; (J) LUDI; (K) PLP; (L) PMF; (M) XSCORE.

In this study, we tested our QM-based-method's ability to discriminate between native and decoy poses for 20 protein targets with bound ligands. The decoy poses and the targets were obtained from the study of Wang et al.,[28] and this data set allowed us to compare our method with available empirical and knowledge-based scoring functions in terms of its ability to detect decoy poses from the experimental "pose". The success of any scoring function in predicting the correct binding mode can be judged by the following set of criteria: (a) A physically based scoring function will describe a funnel-shaped binding free energy surface, where poses that are conformationally distant from the native binding mode will have poorer scores compared to those that are closer to the native. (b) Ideally the native binding mode (determined by X-ray crystallography in this case) is the global minimum on the free energy surface and will rank first among a set of decoys. (c) The root-mean-squared deviation (rmsd) from the native pose of the top-scoring poses will be small. We tested the first criterion by calculating the correlation coefficient (R) between the scores and the rmsd for 20 protein−ligand complexes, using TotalScore and 11 other scoring functions. The average R for the set of 20 protein−ligand complexes for TotalScore1 is 0.58, which is second only to XScore (an empirical scoring function developed by Wang et al. and specifically parametrized against this set). TotalScore1 here is the unweighted sum of all the parts of the master equation, while in TotalScore2 the weight of the gas-phase electrostatic interaction is doubled in order to investigate the importance of electrostatic interactions in binding. The average correlation coefficient for TotalScore2 increases to 0.59, thus highlighting the importance of electrostatics (Figure 9).

Another criterion for the success of any scoring function is its ability to rank the native pose as the best pose. Native poses in most cases is an X-ray crystal structure, which is thought of as the global minimum energy conformation of the ligand in the active site of the protein. In Table 2 we have listed the rank of the

Table 2. Performance of TotalScore in Discriminating Native from "Decoy Poses" for 20 Protein−Ligand Complexes[a]

	TotalScore1			TotalScore2		
PDB code	native rank	rmsd best rank	av rmsd[b]	native rank	rmsd best rank	av rmsd[b]
1abf	3	0.29	5.91	2	0.29	5.91
1apt	1	0.00	1.70	1	0.00	3.37
1bbz	5	14.03	6.06	1	0.00	5.14
1bhf	1	0.00	2.38	1	0.00	4.80
1bra	2	0.66	0.74	1	0.00	0.61
1cla	7	7.66	4.90	3	7.66	4.00
1drf	16	6.09	5.40	13	7.57	5.59
1fkb	1	0.00	0.99	1	0.00	1.22
1hvr	1	0.00	3.05	1	0.00	3.09
1mnc	9	7.92	5.85	1	0.00	2.00
1ppc	5	8.69	7.53	1	0.00	5.36
2pk4	1	0.00	7.18	1	0.00	4.28
2qwd	7	0.93	3.63	6	0.93	1.35
3cla	4	2.35	7.55	2	2.35	7.25
3fx2	1	0.00	1.87	1	0.00	1.62
3ptb	3	1.87	1.38	2	1.87	1.38
5cna	5	3.40	3.26	1	0.00	2.75
5sga	5	8.02	4.71	1	0.00	2.77
7est	3	3.53	2.74	1	0.00	2.18
1tni	8	5.20	3.92	10	15.19	5.45

[a] TotalScore1 is the raw score calculated as the sum of all contributions. In TotalScore2 the weight of the electrostatic interaction is doubled. [b] Average rmsd is the average root-mean-squared deviation of the top five scoring poses.

native binding mode based on TotalScore for the 20 protein−ligand complexes that we studied. For 14 of the 20 complexes the native rank is in the top 5 with TotalScore1, and 16 of 20 complexes rank in the top 5 for TotalScore2. The average rank of the native pose is 4 and 3 for TotalScore1 and TotalScore2, respectively.

The absolute rank of the native pose is a very stringent criterion for success because it is possible that the native binding mode is the average conformation of an ensemble population of binding modes in the active site. Hence, we also report the rmsd of the best scoring pose for the 20 complexes. If the native binding mode is representative of a population of conformationally similar binding modes, then the rmsd for the best scoring pose should not be very large when compared with that for the native structure. The average rmsd for the best-ranked pose from the native pose is 3.76 for TotalScore1 and 1.92 for TotalScore2. For further insight, we also report the average rmsd of the 5 top ranking poses using TotalScore1 and TotalScore2, which is 3.94 and 3.38, respectively. The importance of specific electrostatic interactions is shown to be very important in TotalScore2 where doubling the weight of the electrostatic interaction results in better discrimination of native or native-like poses from decoys. This effect is more pronounced in some complexes such as human plasminogen kringle 4 and ϵ-aminocaproic acid complex (PDB code 2PK4) and the neuraminidase inhibitor complex (PDB code 2QWD). In the ϵ-aminocaproic acid complex, R increases from 0.004 to 0.46, and in the neuraminidase inhibitor complex, R increases from 0.67 to 0.8 when we double the electrostatic interaction weight.

To emphasize the importance of electrostatics in recognition, Figure 10 shows the ability of the gas-phase electrostatic part of TotalScore or heat of interaction (ΔH_I) to discriminate between the native and decoy poses for these two complexes. The key hydrogen-

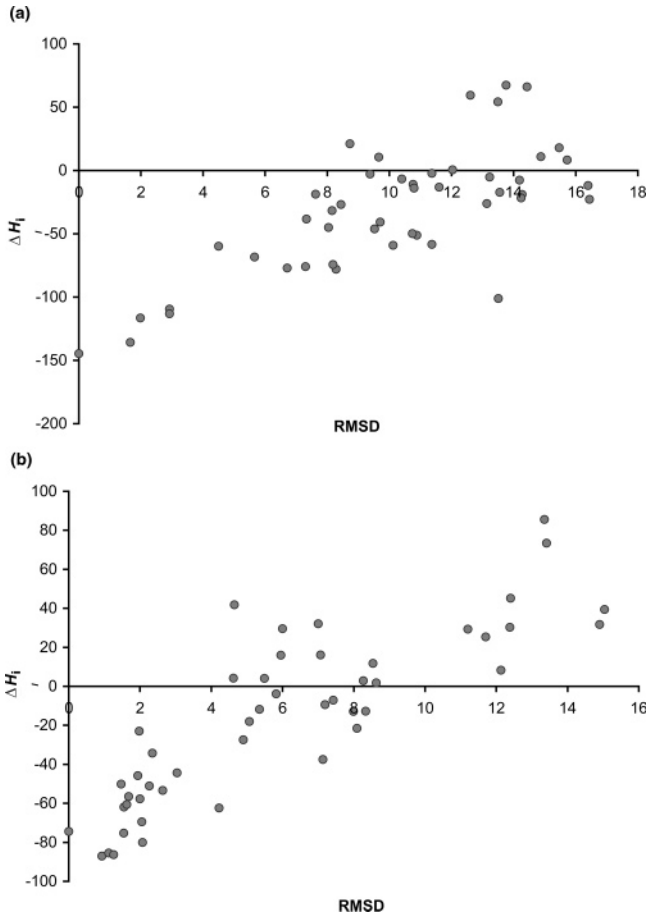

Figure 10. (a) Heat of interaction (ΔH_I) in kcal/mol versus root-mean-squared deviation in angstroms between native and decoy poses for ϵ-aminocaproic acid−human plasminogen kringle 3 complex. (b) Heat of interaction (ΔH_I) in kcal/mol versus root-mean-squared deviation in angstroms between native and decoy poses for the neuraminidase inhibitor complex.

bonding and salt-bridge interactions between the ligand and the protein are critical in the native binding pose for the ϵ-aminocaproic acid and neuraminidase inhibitor. Loss of these interactions presumably in the decoy structures leads to loss of specific electrostatic interactions that define the native binding mode. The ΔH_I is successful in capturing these interactions and by itself is capable of discriminating native from decoys. For ϵ-aminocaproic acid, ΔH_I scores the native binding mode as the best pose, whereas in case of the neuraminidase inhibitor, the best pose has a 0.93 Å rmsd from the native structure. This pose is conformationally very close to the native binding mode and is involved in all the key hydrogen bond and salt-bridge interactions with the protein.

The ability to discriminate native poses from decoy poses implies that the scoring function can capture the salient features of the binding free energy surface of a protein−ligand complex and can distinguish between false or local minima and true global minima. Our conclusions from these results can be interpreted in light of the funnel theory of protein folding and protein−ligand interaction.[83,84] The search for the binding site on the protein surface can be thought of as a phenomenon, which is driven by macroscopic or long-range effects such as solvent entropy and electrostatic desol-

vation. The exclusion of water from the active site during protein−ligand interaction approximated by surface area burial during binding can coarsely discriminate native-like ligands from decoy poses. However, regiospecific electrostatic and steric interactions in the active site between the ligand and protein can fine-tune the final discrimination of the protein for a specific ligand. This is observed in our studies as well.

Charge Analysis. QM calculations on protein−ligand complexes provide us with an opportunity to study the distribution of formal charges on the amino acid residues in the protein. In nonpolarizable force fields the formal charges are assigned a constant value on the basis of the physiological pH. For example, Asp and Glu are modeled as acidic residues with −1 charge, whereas Lys and Arg are modeled as basic residues with a +1 formal charge. All other residues are modeled as neutral residues with 0 formal charge. The N and C termini residues are assigned +1 and −1 formal charges. However, it is well-known that the electron density is perturbed in response to the environment as well as in response to the solvent reaction field. Hence, point charges on similar atom types depend on the environment they are in. These point charges can be influenced by the protein (core) and the solvent (surface) environment and thus lead to a distribution of formal charges on amino acid residues that are different from force field assigned charges.

We analyzed the formal charges on all 20 amino acid residues in the 165 proteins for which we calculated the solute wave function using the semiempirical Hamiltonian AM1 and the PB/SCRF method. These amino acids were divided into core, boundary, and surface residues based on the percentage of surface area exposed. Surface areas were calculated with the SASA program[55] using a solvent probe radius of 1.4 Å. The core residues were 0−35% exposed to solvent, boundary residues were 35−75% exposed to solvent, and surface residues were 75−100% exposed to solvent. The charged N and C termini and amino acids were removed from this analysis. The results of this analysis are reported in Table SIV of the Supporting Information. For hydrophobic residues such as valine, leucine, isoleucine, etc., the number of exposed residues on the surface was not statistically significant for such an analysis. Hence, in those cases we have reported the distribution just for the core and boundary residues. For acidic residues such as aspartates and glutamates, we find the average charge to be dependent on their location in the protein. For example, the average charge on the Asp in the core of the protein is −0.93 (SD = 0.04) while surface residues are closer to −1.0. Similarly for Glu, the average charge on the residues found in the core is −0.94 (SD = 0.06), whereas on the surface the average charge is −1.033 (SD = 0.2). For basic residues such as Lys the average charge on core residues is 0.97 (SD = 0.03), while surface residues have an average charge of 0.98 (SD = 0.02). Arg shows similar trends where the average charge increases from 0.95 to 0.99 from core to the surface of the protein. The standard deviation of the charges from the average value in general is higher for residues found in the core of the protein than for those found on the surface. This highlights the importance polarization in the heterogeneous protein environment.

In general, the standard deviation from the average formal charge for the surface residues is lower when compared to that for core residues. This is likely due to the homogeneous solvent environment around exposed residues, although it should be kept in mind that there is a distinct possibility of charge transfer between the surface residues and explicit solvent if it is accounted for in such calculations.[20,86] Other interesting trends can be noted from this analysis. For example, on average, Pro, His, Met, Asp, Glu, Ser, Thr, and Tyr residues have slightly negative formal charges at the core, boundary, and surface regions of the protein. However, the standard deviations from the average charges in all these cases are greater in magnitude from the average itself, implying formal charges on these residues are highly dependent on the environment they are in. Hydrophobic residues such as Phe, Ala, Leu, Ile, and Val have slightly positive formal charges in core regions of the protein, while in boundary regions they have slightly negative or positive formal charges (surface residues for these amino acids were not present in statistically significant numbers). The standard deviations in all these cases point toward a significant spread of the formal charges in different environments in proteins.

In our previous work we have shown the importance of charge transfer (CT) in biomolecular interactions.[20,86] We have also demonstrated CT in protein−ligand interaction during zinc-mediated ligand binding in metalloenzymes.[22] In this study we undertook a global analysis of CM2 CT in protein−ligand interactions. The charge transferred between the protein and the ligand for the 165 noncovalent protein−ligand complexes from our validation set was analyzed. The results are plotted in Figure S2 in Supporting Information as a frequency distribution for protein−ligand complexes in a specific CT bin. The positive CT bins consist of protein−ligand complexes in which charge is transferred from the ligand to the protein, whereas negative CT bins consist of complexes in which charge is transferred from the protein to the ligand. The frequency distribution of protein−ligand complexes reveals that 24% of complexes lie in the CT bin of −0.01 to 0.01 electrons. For the rest, greater than 0.01 electrons are being transferred either from the ligand to the protein or from the protein to the ligand. Notably, 61% of the proteins transfer charge to the ligand, whereas 39% of ligands transfer charge to the protein. A statistically significant number of ligands (11%) transfer greater than 0.1 electron to the protein, whereas a less significant number of proteins (4%) transfer greater than 0.1 electron to the ligand. For CT from the protein to the ligand, there is more of a spread among different CT bins resembling a normal distribution, whereas CT from ligand to the protein is dominated by 12% of complexes in the 0.0−0.01 bin and 11% of the complexes in the greater than 0.1 bin. We have listed CT for Mulliken, CM1, and CM2 charges for all 165 complexes in Table SI of Supporting Information.

We also analyzed charge transfer in 40 metalloenzymes such as human carbonic anhydrase II (HCAII), carboxypeptidase (CPA), and matrix metalloproteases (MMP) in this study. The metal atoms in these protein−ligand complexes were treated as a part of the protein. Compared to noncovalent complexes, not surprisingly, there is more charge transferred between proteins and

the bound ligands in metalloenzymes. In HCAII the average CM2 CT is −1.01 electron (SD = 0.15 e^-). In CPA the average CT is −0.62 electron (SD = 0.09 e^-), and in MMP the average CT is 0.44 electron (SD = 0.38 e^-). Interestingly, in MMPs, charge is being transferred from the ligand to the protein, whereas in HCAII and CPA it being transferred from the protein to the ligands. Mulliken, CM1, and CM2 CT for the 40 metalloproteins is listed in Table SII of Supporting Information.

Overall, these observations demonstrate the challenges faced by nonpolarizable fixed-point charge models that are routinely used to model protein−ligand interaction. Importantly, the amount of CT is variable in magnitude and direction, which makes it very important to include it in a scoring model because it may make a difference in whether a compound is flagged as inactive or active and whether CT (and polarization) is accounted for correctly. The transfer of charge between the ligand and protein and the dependence of formal charges on the environment can alter the nature of the electrostatic interaction between the ligand and the protein, and hence, fixed-point charge models represent a relatively severe approximation.

Conclusions

In this work we report the development of the first-generation quantum mechanics based scoring function for predicting the binding affinity and binding mode of protein−ligand complexes. Our approach to calculating binding free energy is promising and shows inherent predictive capability. We have shown this approach to be successful in capturing binding free energy trends in a diverse set of protein−ligand complexes without having to fit different contributions to the experimental observations. There are precious few studies in the literature that assess performance of binding free energy prediction on a diverse data set that are not fit to or derived from experiments. However, we note that using QMScore, predictive models can be constructed for different protein families by fitting our scoring function to experimental binding free energies. We have shown the predictive power of such models in calculating the binding free energy from an experimental structure solved by X-ray crystallography and also from poses that have been docked in the active site using a docking program. Understandably, within protein families the agreement we observe with experiment is better. In fact, in structure-based virtual design the predictive capability of a scoring function within protein families is of more practical value than across protein families.

In the second part of this study, we demonstrated the ability of this quantum mechanics based scoring function to discriminate between native and decoy poses. Although the size of this data set is not large in our study (because of computational time considerations), the general trend points toward the ability of this scoring function to discriminate between native and decoy poses. We further demonstrate the importance of electrostatics in discrimination, especially in polar protein−ligand complexes. When the weight of the electrostatic interaction is doubled, the discriminatory power of the scoring function increases. Our results are in agreement with other studies in the literature[87−90] that underline the importance of electrostatic interactions in determining the specificity of the binding mode and, hence, in discriminating native from decoy poses.

In this work we have also demonstrated that the power of quantum mechanics can be extended to a detailed study of protein−ligand interactions with relatively modest computational resources. For an average size protein−ligand complex, our linear scaling D&C program can calculate the gas-phase and solvated wave function in 4 h on a 1.8 GHz AMD Athlon machine with a 1 GB RAM. We envision such calculations to be routinely used in the near future because of the advent of new algorithms and technologies and the falling cost of computer hardware. The advantage of using QM Hamiltonians is that they obviate the need to determine atom types in different chemical environments, traditionally used in scoring functions. And also effects such as polarization and charge transfer, especially between metal ions and betweem the protein and the ligand, are better captured. These effects are not pairwise additive and are beyond the scope of classical potentials. This study sets the stage for large-scale application of quantum mechanics to problems of biological interest.

In terms of performance and predictive ability, there is certainly scope for further improvement in the scoring scheme and the Hamiltonians themselves. Although our quantum mechanics based scoring function outperforms other scoring functions in the literature, we realize that the agreement with experiments for both binding affinity and binding mode leaves a lot to be desired. Uncertainties in structure determination[43] as well as in experimental measurements[91] can be one cause of poor performance. The role of electrostatics and its effects on pK_a values of ionizable groups in the active site has been ignored in this study as well as other scoring functions in the literature. Ionizable groups in the active site with perturbed pK_a values can have a significant effect on the interaction energy.[92] Scoring functions also ignore the role of water molecules during binding in validation studies from X-ray crystallographic structures. The microscopic interactions of solvent with the protein and ligand can influence the strength of the interaction and should be taken into consideration in scoring. This is especially important when water forms hydrogen bond networks within the active site in protein−ligand complexes.[93]

The assumption of one dominant binding mode of the ligand (X-ray crystal mode or a docking pose) in these calculations is a poor assumption.[94,95] In the case of docking, use of simplistic potentials for determination of the binding mode may itself be a source of uncertainty. A simple potential might misrepresent the binding free energy surface, but sampling with physically based potentials is presently computationally intractable, and it is also not clear if they would lead to convergent solutions in every case. These are some of the vexing problems associated with finding the correct binding mode for a ligand in the active site. In our future work we hope to address these issues and to improve the predictive power of our scoring function. Indeed, we envision that an accurate quantum mechanics based scoring function will be routinely used to determine the binding free energy of small molecules bound to diverse protein targets. This will prove to be a significant development in the field of scoring and will be used as

a powerful tool in the process of lead optimization, a critical and challenging part of drug discovery.

Acknowledgment. We thank the NSF (Grant MCB-0211639) and NIH (Grant GM 44974) for generous support of this work and National Center for Supercomputer Applications (NCSA) and Pittsburgh Supercomputer Center (PSC) for computer resources. We thank Kate Holloway for the HIV-1 protease inhibitor coordinates and Michael Jacobsson for the coordinates and binding affinity data of inhibitors bound to MMP3.

Supporting Information Available: Tables listing PDB codes, experimental free energy of binding, charge transfer, proton affinity, and charges; figures showing the effect of soft-core constants and the frequency distribution of charge transfer. This material is available free of charge via the Internet at http://pubs.acs.org.

References

(1) Drews, J. Drug Discovery: A Historical Perspective. *Science* **2000**, *287*, 1960−1964.
(2) Good, A. Structure-Based Virtual Screening Protocols. *Curr. Opin. Drug Discovery Dev.* **2001**, *4*, 301−307.
(3) Jorgensen, W. L. The Many Roles of Computation in Drug Discovery. *Science* **2004**, *303*, 1813−1818.
(4) Halperin, I.; Buyong, M.; Wolfson, H.; Nussinov, R. Principles of Docking: An Overview of Search Algorithms and a Guide to Scoring Functions. *Proteins: Struct., Funct., Genet.* **2002**, *47*, 409−443.
(5) Dixon, J. S. Evaluation of the CASP2 Docking Section. *Proteins: Struct., Funct., Genet.* **1997**, Suppl. 1, 198−204.
(6) Diller, D. J.; Verlinde, C. L. Critical Evaluation of Several Global Optimization Algorithms for the Purpose of Molecular Docking. *J. Comput. Chem*. **1999**, *20*, 1740−1751.
(7) Gilson, M. K.; Given, J. A.; Head, M. S. A New Class of Models for Computing Receptor−Ligand Affinities. *Chem. Biol.* **1997**, *4*, 87−92.
(8) Schneidman-Duhovny, D.; Nussinov, R.; Wolfson, H. J. Predicting Molecular Interactions in Silico: II. Protein−Protein and Protein−Drug Docking. *Curr. Med. Chem.* **2004**, *11*, 91−107.
(9) Kollman, P. A. Free Energy Calculations. Applications to Chemical and Biological Phenomenon. *Chem. Rev.* **1993**, *7*, 2395−2417.
(10) Raha, K.; Merz, K. M., Jr. Calculating Binding Free Energy in Protein−Ligand Interaction. *Annu. Rep. Comput. Chem.*, in press.
(11) Dixon, S. L.; Merz, K. M., Jr. Semiempirical Molecular Orbital Calculations with Linear System Size Scaling. *J. Chem. Phys.* **1996**, *104*, 6643−6649.
(12) Dixon, S. L.; Merz, K. M., Jr. Fast, Accurate Semiempirical Molecular Orbital Calculations for Macromolecules. *J. Chem. Phys.* **1997**, *107*, 879−893.
(13) van der Vaart, A.; Gogonea, V.; Dixon, S. L.; Merz, K. M., Jr. Linear Scaling Molecular Orbital Calculations of Biological Systems Using the Semiempirical Divide and Conquer Method. *J. Comput. Chem.* **2000**, *21*, 1494−1504.
(14) Dixon, S. L.; van der Vaart, A.; Gogonea, V.; Vincent, J. J.; Brothers, E. N.; et al. *DivCon*; The Pennsylvania State University: University Park, PA, 1999.
(15) Dewar, M. J. S.; Zoebisch, E. G.; Healy, E. F.; Stewart, J. J. P. AM1: A New General Purpose Quantum Mechanical Molecular Model. *J. Am. Chem. Soc.* **1985**, *107*, 3902−3909.
(16) Cramer, C. J.; Truhlar, D. G. PM3-SM3: A General Parametrization for Including Aqueous Solvation Effects in the PM3 Molecular Orbital Method. *J. Comput. Chem.* **1992**, *12*, 1089−1097.
(17) Dewar, M. J. S.; Thiel, W. Ground States of Molecules. 38. The MNDO Method. Approximations and Parameters. *J. Am. Chem. Soc.* **1977**, *99*, 4899−4907.
(18) Thiel, W.; Voityuk, A. A. Extension of MNDO to d Orbitals: Parameters and Results for the Second-Row Elements and for the Zinc Group. *J. Phys. Chem.* **1996**, *100*, 616−626.
(19) Repasky, M. P.; Chandrasekhar, J.; Jorgensen, W. L. PDDG/PM3 and PDDG/MNDO: Improved Semiempirical Methods. *J. Comput. Chem.* **2002**, *23*, 1601−1622.
(20) van der Vaart, A.; Merz, K. M., Jr. The Role of Polarization and Charge Transfer in the Solvation of Biomolecules. *J. Am. Chem. Soc.* **1999**, *121*, 9182−9190.
(21) Perez, C.; Ortiz, A. R. Evaluation of Docking Functions for Protein−Ligand Docking. *J. Med. Chem*. **2001**, *44*, 3786−3785.
(22) Raha, K.; Merz, K. M., Jr. A Quantum Mechanics Based Scoring Function: Study of Zinc-Ion Mediated Ligand Binding. *J. Am. Chem. Soc.* **2004**, *126*, 1020−1021.
(23) Nikitina, E.; Sulimov, D.; Zayets, V.; Zaitseva, N. Semiempirical Calculations of Binding Enthalpy for Protein−Ligand Complexes. *Int. J. Quantum Chem.* **2004**, *97*, 747−763.
(24) Vasilyev, V.; Bliznyuk, A. A. Application of Semiempirical Quantum Chemical Methods as a Scoring Function in Docking. *Theor. Chem. Acc.* **2004**, *112*, 313−317.
(25) Bohm, H. J. The Development of a Simple Empirical Scoring Function To Estimate the Binding Constant for a Protein−Ligand Complex of Known Three-Dimensional Structure. *J. Comput.-Aided Mol. Des.* **1994**, *8*, 243−256.
(26) DeWitte, R. S.; Shakhnovich, E. I. De Novo Design Method Based on Simple, Fast and Accurate Free Energy Estimates. 1. Methodology and Supporting Evidence. *J. Am. Chem. Soc.* **1996**, *118*, 11733−11744.
(27) Wang, T.; Wade, R. C. Comparative Binding Energy (COMBINE) Analysis of OppA-Peptide Complexes To Relate Structure to Binding Thermodynamics. *J. Med. Chem*. **2002**, *45*, 4828−4837.
(28) Wang, R.; Lu, Y.; Wang, S. Comparative Evaluation of 11 Scoring Functions for Molecular Docking. *J. Med. Chem*. **2003**, *46*, 2287−2303.
(29) Kurinov, I. V.; Harrison, R. W. Prediction of New Serine Proteinase Inhibitors. *Nat. Struct. Biol.* **1994**, *1*, 735−743.
(30) Stubbs, M. T.; Huber, R.; Bode, W. Crystal Structure of Factor Xa Specific Inhibitors in Complex with Trypsin: Structural Grounds for Inhibition of Factor Xa and Selectivity against Thrombin. *FEBS Lett.* **1995**, *375*, 103−107.
(31) Hunenberger, P. H.; Helms, V.; Narayana, N.; Taylor, S. S.; McCammon, J. A. Determinants of Ligand Binding to cAMP-Dependent Protein Kinase. *Biochemistry* **1999**, *38*, 2358−2366.
(32) Zhao, B.; Bower, M. J.; McDevitt, P. J.; Zhao, H.; Davis, S. T.; et al. Structural Basis for Chk1 Inhibition by UCN-01. *J. Biol. Chem.* **2002**, *277*, 46609−46615.
(33) Burkhard, P.; Tylor, P.; Walkinshaw, M. D. X-ray Structures of Small Ligand−FKBP Complexes Provide an Estimate for Hydrophobic Interaction Energies. *J. Mol. Biol.* **2000**, *295*, 953−962.
(34) Charifson, P. S.; Shewchuck, L. M.; Rocque, W.; Hummel, C. W.; Jordan, S. R.; et al. Peptide Ligands of pp60c-src SH2 Domains: A Thermodynamic and Structural Study. *Biochemistry* **1997**, *36*, 6283−6293.
(35) Dullweber, F. D.; Stubbs, M. T.; Musil, D.; Sturzebecher, J.; Klebe, G. Factorising Ligand Affinity: A Combined Thermodynamic and Crystallographic Study of Trypsin and Thrombin Inhibition. *J. Mol. Biol.* **2001**, *313*, 593−614.
(36) Jacobsson, M.; Liden, P.; Strenschantz, E.; Bostrom, H.; Norinder, U. Improving Structure-Based Virtual Screening by Multivariate Analysis of Scoring Data. *J. Med. Chem*. **2003**, *46*, 5781−5789.
(37) *SYBYL*, version 6.8; Tripos Inc.: St. Louis, MO.
(38) *Cerius2*, version 4.6; Accelrys Inc.: San Diego, CA.
(39) James, M. N. G.; Sielecki, A. R.; Brayer, G. D.; Delbaere, L. T. J. Structures of Product and Inhibitor Complexes of *Streptomyces griseus* Protease A at 1.8 Angstrom Resoultion. *J. Mol. Biol.* **1980**, *144*, 43−88.
(40) Case, D. A.; Caldwell, J. W.; Cheatham, T. E., II; Ross, W. S.; Simmerling, C. L.; et al. *AMBER*, version 5.0; University of California: San Francisco.
(41) Walters, W. P. J.; Stahl, M. *BABEL*, version 1.6; The University of Arizona: Tucson, AZ.
(42) van Aalten, D. M. F.; Bywater, R.; Findlay, J. B. C.; Hendlich, M.; Hooft, R. W. W.; et al. PRODRG, a Program for Generating Molecular Topologies and Unique Molecular Descriptors from Coordinates of Small Molecules. *J. Comput.-Aided Mol. Des.* **1996**, *10*, 255−262.
(43) Nissink, J. W. M.; Murray, C. W.; Hartshorn, M.; Verdonk, M. L.; Cole, J. C.; et al. A New Test Set for Validating Predictions of Protein−Ligand Interactions. *Proteins: Struct., Funct., Genet.* **2002**, *49*, 457−471.
(44) Stewart, J. J. P. *Semiempirical Molecular Orbital Methods*; VHC: New York, 1990; pp 313−365.
(45) Stone, A. J. *The Theory of Intermolecular Forces*; Clarendon: Oxford, 1996.
(46) Sinnokrot, M. O.; Valeev, E. F.; Sherrill, C. D. Estimates of the ab Initio Limit for $\pi-\pi$ Interactions: The Benzene Dimer. *J. Am. Chem. Soc.* **2002**, *124*, 10887−10893.
(47) Kristyan, S.; Pulay, P. Can (Semi) Local Density Functional Theory Account for London Dispersion Forces? *Chem. Phys. Lett.* **1994**, *229*, 175−180.
(48) Cornell, W. D.; Cieplak, P.; Baylay, C. I.; Gould, I. R.; Merz, K. M., Jr.; et al. A Second Generation Force Field for the Simulation of Proteins, Nucleic Acids, and Organic Molecules. *J. Am. Chem. Soc.* **1995**, *117*, 5179−5197.
(49) Murray, C. W.; Verdonk, M. L. The Consequences of Translational and Rotational Entropy Lost by Small Molecules on Binding to Proteins. *J. Comput.-Aided Mol. Des.* **2002**, *16*, 741−753.

(50) Schwarzl, S. M.; Tschopp, T. B.; Smith, J. C.; Fischer, S. Can the Calculation of Ligand Binding Free Energies Be Improved with Continuum Solvation Electrostatics and an Ideal-Gas Entropy Correction. *J. Comput. Chem.* **2002**, *23*, 1143−1149.
(51) Bardi, J. S.; Luque, I.; Freire, E. Structure-Based Thermodynamic Analysis of HIV-1 Protease Inhibitors. *Biochemistry* **1997**, *36*, 6588−6596.
(52) Vajda, S.; Weng, Z.; Rosenfeld, R.; DeLisi, C. Effect of Conformational Flexibility and Solvation on Receptor−Ligand Binding Free Energies. *Biochemistry* **1994**, *33*, 13977−13988.
(53) Ishchenko, A. V.; Shakhnovich, E. I. Small Molecule Growth 2001 (SMoG2001): An Improved Knowledge-Based Scoring Function for Protein−Ligand Interactions. *J. Med. Chem.* **2002**, *43*, 2770−2780.
(54) Eldridge, M. D.; Murray, C. W.; Auton, T. R.; Paolini, G. V.; Mee, R. P. Empirical Scoring Functions: I. The Development of a Fast Empirical Scoring Function To Estimate the Binding Affinity of Ligands in Receptor Complexes. *J. Comput.-Aided Mol. Des.* **1997**, *11*, 425−445.
(55) LeGrand, S. M.; Merz, K. M., Jr. Rapid Approximation to Molecular Surface Area via the Use of Boolean Logic and Look-Up Tables. *J. Comput. Chem.* **1993**, *14*, 349−352.
(56) Kuhn, B.; Kollman, P. A. Binding of a Diverse Set of Ligands to Avidin and Streptavidin: An Accurate Quantitative Prediction of Their Relative Affinites by Combination of Molecular Mechanics and Continuum Solvation Models. *J. Med. Chem.* **2000**, *43*, 3786−3791.
(57) Zhou, R.; Friesner, R. A.; Ghosh, A.; Rizzo, R. C.; Jorgensen, W. L.; et al. New Linear Interaction Method for Binding Affinity Calculations Using Continuum Solvation Model. *J. Phys. Chem. B* **2001**, *105*, 10388−10397.
(58) Zou, X.; Sun, Y.; Kuntz, I. D. Inclusion of Solvation in Ligand Binding Free Energy Calculations Using the Generalized-Born Model. *J. Am. Chem. Soc.* **1999**, *121*, 8033−8043.
(59) Gogonea, V.; Merz, K. M., Jr. Fully Quantum Mechanical Description of Proteins in Solution. Combining Linear Scaling Quantum Mechanical Methodologies with the Poisson−Boltzmann Equation. *J. Phys. Chem. A* **1999**, *103*, 5171−5188.
(60) Gogonea, V.; Suarez, D.; van der Vaart, A.; Merz, K. W. New Developments in Applying Quantum Mechanics to Proteins. *Curr. Opin. Struct. Biol.* **2001**, *11*, 217−223.
(61) Luque, F. J.; Curutchet, C.; Munoz-Muriedas, J.; Bidon-Chanal, A.; Soteras, I.; et al. Continuum Solvation Models: Dissecting the Free Energy of Solvation. *Phys. Chem. Chem. Phys.* **2003**, *5*, 3827−3836.
(62) Gogonea, V.; Merz, K. M., Jr. Charge Flow between Ions and a Dielectric Continuum. Variational Method for Distributing Charge into the Dielectric. *J. Phys. Chem. B* **2000**, *104*, 2117−2122.
(63) Verkhiver, G. M.; Rejto, P. A.; Bouzida, D.; Arthurs, S.; Colson, A. B.; et al. Towards Understanding the Mechanisms of Molecular Recognition by Computer Simulation of Ligand−Protein Interactions. *J. Mol. Recognit.* **1999**, *12*, 371−389.
(64) Head, R. D.; Smythe, M. L.; Opera, T. I.; Waller, C. L.; Green, S. M.; et al. VALIDATE: A New Method for the Receptor-Based Prediction of Binding Affinities of Novel Ligands. *J. Am. Chem. Soc.* **1996**, *118*, 3959−3969.
(65) Opera, T. I.; Marshall, G. R. Receptor Bases Prediction of Binding Affinities. *Perspect. Drug Discovery Des.* **1998**, *9*, 35−61.
(66) Jain, A. Scoring Non-Covalent Protein−Ligand Interactions: A Continuous Differentiable Function Tuned To Compute Binding Affnities. *J. Comput.-Aided Mol. Des.* **1996**, *10*, 427−440.
(67) Babine, R. E.; Bender, S. L. Molecular Recognition of Protein−Ligand Complexes: Applications to Drug Design. *Chem. Rev.* **1997**, *87*, 1359−1472.
(68) Miller, M.; Schneider, J.; Sathyanarayana, B. K.; Toth, M. V.; Marshall, G. R.; et al. Structure of complex of synthetic HIV-1 protease with a substrate-based inhibitor at 2.3 Å resolution. *Science* **1989**, *246*, 1149−1152.
(69) Muegge, I.; Martin, Y. C. A General and Fast Scoring Function for Protein−Ligand Interactions: A Simplified Potential Approach. *J. Med. Chem.* **1999**, *42*, 791−804.
(70) Holloway, M. K.; Wai, J. M.; Halgren, T. A.; Fitzgerald, P. M. D.; Vacca, J. P.; et al. A Priori Prediction of Activity for HIV-1 Protease Inhibitors Employing Energy Minimization in the Active Site. *J. Med. Chem.* **1995**, *38*, 305−317.
(71) Hyland, L. J.; Tomaszek, T. A.; Meek, T. D. Human Immunodeficiency Virus-1 Protease. 2. Use of pH Rate Studies and Solvent Kinetic Isotope Effects To Elucidate Details of Chemical Mechanism. *Biochemistry* **1991**, *30*, 8454−8563.
(72) Spyrakis, F.; Fornabaio, M.; Cozzini, P.; Mozzarelli, A.; Abraham, D. J.; et al. Computational Titration Analysis of a Multiprotic HIV-1 Protease−Ligand Complex. *J. Am. Chem. Soc.* **2004**, *126*, 11764−11765.
(73) Rajamani, R.; Reynolds, C. H. Modeling the Protonation States of Catalytic Aspartates in β-Secretase. *J. Med. Chem.* **2004**, *47*, 5159−5166.
(74) Muegge, I. A Knowledge-Based Scoring Function for Protein−Ligand Interaction: Probing the Reference State. *Perspect. Drug Discovery Des.* **2000**, *20*, 99−114.
(75) Ma, B.; Shatsky, M.; Wolfson, H. J.; Nussinov, R. Multiple Diverse Ligands Binding at a Single Protein Site: A Matter of Pre-existing Populations. *Protein Sci.* **2001**, *11*, 184−197.
(76) Ewing, T.; Kuntz, I. D. Critical Evaluation of Search Algorithms for Automated Molecular Docking and Database Screening. *J. Comput. Chem.* **1997**, *18*, 1175−1189.
(77) Goodsell, D. S.; Olson, A. J. Automated Docking of Substrates to Proteins by Simulated Annealing. *Proteins: Struct., Funct., Genet.* **1990**, *8*, 195−202.
(78) Abagyan, R. A.; Totrov, M. M.; Kuznetsov, D. N. ICM−A New Method for Protein Modelling and Design. Applications to Docking and Structure Prediction from the Distorted Native Conformation. *J. Comput. Chem.* **1994**, *15*, 488−506.
(79) Halgren, T. A. Merck Molecular Force Field: 1. Basis, Form, Scope, Parameterization, and Performance of MMFF94. *J. Comput. Chem.* **1996**, *17*, 490−519.
(80) Ferrari, A. M.; Wei, B. Q.; Costantino, L.; Shoichet, B. K. Soft Docking and Multiple Receptor Conformations in Virtual Screening. *J. Med. Chem.* **2004**, *47*, 5076−5084.
(81) Fernandez-Recio, J.; Totrov, M.; Abagyan, R. Soft Protein−Protein Docking in Internal Coordinates. *Protein Sci.* **2002**, *11*.
(82) Vieth, M.; Hirst, J. D.; Kolinski, A.; Brooks, C. L., III. Assessing Energy Funtions in Flexible Docking. *J. Comput. Chem.* **1998**, *19*, 1612−1622.
(83) Onuchic, J. N.; Wolynes, P. G. Theory of Protein Folding. *Curr. Opin. Struct. Biol.* **2004**, *14*, 70−75.
(84) Camacho, C. J.; Weng, Z.; Vajda, S.; DeLisi, C. Free Energy Landscapes of Encounter in Protein−Protein Association. *Biophys. J.* **1999**, *76*, 280−291.
(85) Rarey, M.; Kramer, B.; Lengauer, T.; Klebe, G. A Fast Flexible Docking Method Using an Incremental Construction Algorithm. *J. Mol. Biol.* **1996**, *261*, 470−489.
(86) van der Vaart, A.; Merz, K. M., Jr. Charge Transfer in Biologically Important Molecules: Comparison of High-Level ab Initio and Semiempirical Methods. *Int. J. Quantum Chem.* **2000**, *77*, 27−43.
(87) Camacho, C. J.; Gatchell, D. W.; Kimura, S. R.; Vajda, S. Scoring Docked Conformations Generated by Rigid-Body Protein−Protein Docking. *Proteins: Struct., Funct., Genet.* **2000**, *40*, 525−537.
(88) Jakoby, M. G.; Miller, K. R.; Toner, J. J.; Bauman, A.; Cheng, L.; et al. Ligand−Protein Electrostatic Interactions Govern the Specificity of Retinol and Fatty Acid-Binding Proteins. *Biochemistry* **1993**, *32*, 872−878.
(89) Hendsch, Z. S.; Tidor, B. Do Salt Bridges Stabilize Proteins? A Continuum Electrostatic Analysis. *Protein Sci.* **1994**, *3*, 211−226.
(90) Hendsch, Z. S.; Tidor, B. Electrostatic Interactions in the GCN4 Leucine Zipper: Substantial Contributions Arise from Intramoleculer Interactions Enhanced on Binding. *Protein Sci.* **1999**, *8*, 1381−1392.
(91) Munson, P. J. Experimental Artifacts and Analysis of Ligand Binding Data: Results of a Computer Simulation. *J. Recept. Res.* **1983**, *3*, 249−259.
(92) Kellogg, G. E.; Fornabaio, M.; Spyrakis, F.; Lodola, A.; Cozzini, P.; et al. Getting It Right: Modeling of pH, Solvent, and "Nearly" Everything Else in Virtual Screening of Biological Targets. *J. Mol. Graphics Modell.* **2004**, *22*, 479−486.
(93) Hamelberg, D.; McCammon, J. A. Standard Free Energy of Releasing a Localized Water Molecule from the Binding Pockets of Proteins: Double−Decoupling Method. *J. Am. Chem. Soc.* **2004**, *126*, 7683−7689.
(94) Lukacova, V.; Balaz, S. Multimode Ligand Binding in Receptor Site Modeling: Implementation in CoMFA. *J. Chem. Inf. Comput. Sci.* **2003**, *43*, 2093−2105.
(95) Ota, N.; Agard, D. A. Binding Mode Prediction for a Flexible Ligand in a Flexible Pocket Using Multi-Conformation Simulated Annealing Pseudo Crystallographic Refinement. *J. Mol. Biol.* **2001**, *314*, 607−617.

JM048973N